ACS Partner Journal

CHEM & BIO ENGINEERING

Open Access

pubs.acs.org/ChemBioEng

Review

Review on Blood Flow Dynamics in Lab-on-a-Chip Systems: An Engineering Perspective

Bin-Jie Lai, Li-Tao Zhu, Zhe Chen,* Bo Ouyang,* and Zheng-Hong Luo*

Cite This: *Chem Bio Eng.* 2024, 1, 26−43

Read Online

ACCESS | Metrics & More | Article Recommendations

ABSTRACT: Under different transport mechanisms, blood flow dynamics, heavily linked to the flow shear rate conditions, in "lab-on-a-chip" (LOC) systems are found to result in varying transport phenomena. This Review examines the blood flow patterns in LOC systems through the role of viscoelastic properties such as dynamic blood viscosity and elastic behavior of the red blood cells. The study of blood transport phenomena in LOC systems through key parameters of capillary and electro-osmotic forces is provided through experimental, theoretical, and numerous numerical approaches. The disturbance triggered by electro-osmotic viscoelastic flow is particularly discussed and applied in the enhancement of the mixing and separating capabilities of LOC devices handling blood and other viscoelastic fluids for future research opportunities. Furthermore, the Review identifies the challenges in the numerical modeling of blood flow dynamics under the LOC systems, such as the call for more accurate and simplified blood flow models and the emphasis on numerical studies of viscoelastic fluid flow under the electrokinetic effect. More practical assumptions for zeta potential conditions while studying the electrokinetic phenomena are also highlighted. This Review aims to provide a comprehensive and interdisciplinary perspective on blood flow dynamics in microfluidic systems driven by capillary and electro-osmotic forces.

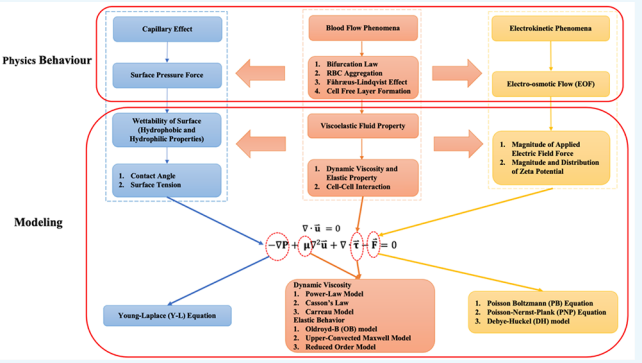

KEYWORDS: *Blood flow, Viscoelastic fluid flow, Numerical Simulation, Capillary Forces, Electro-osmotic flow*

1. INTRODUCTION

1.1. Microfluidic Flow in Lab-on-a-Chip (LOC) Systems. Over the past several decades, the ability to control and utilize fluid flow patterns at microscales has gained considerable interest across a myriad of scientific and engineering disciplines, leading to growing interest in scientific research of microfluidics.[1] Microfluidics, an interdisciplinary field that straddles physics, engineering, and biotechnology, is dedicated to the behavior, precise control, and manipulation of fluids geometrically constrained to a small, typically sub-millimeter, scale.[2] The engineering community has increasingly focused on microfluidics, exploring different driving forces to enhance working fluid transport, with the aim of accurately and efficiently describing, controlling, designing, and applying microfluidic flow principles and transport phenomena, particularly for miniaturized applications.[3] This attention has chiefly been fueled by the potential to revolutionize diagnostic and therapeutic techniques in the biomedical and pharmaceutical sectors

Under various driving forces in microfluidic flows, intriguing transport phenomena have bolstered confidence in sustainable and efficient applications in fields such as pharmaceutical, biochemical, and environmental science. The "lab-on-a-chip" (LOC) system harnesses microfluidic flow to enable fluid processing and the execution of laboratory tasks on a chip-sized scale. LOC systems have played a vital role in the miniaturization of laboratory operations such as mixing, chemical reaction, separation, flow control, and detection on small devices, where a wide variety of fluids is adapted. Biological fluid flow like blood and other viscoelastic fluids are notably studied among the many working fluids commonly utilized by LOC systems, owing to the optimization in small fluid sample volumed, rapid response times, precise control, and easy manipulation of flow patterns offered by the system under various driving forces.[4]

The driving forces in blood flow can be categorized as passive or active transport mechanisms and, in some cases, both. Under various transport mechanisms, the unique design of microchannels enables different functionalities in driving,

Received: August 29, 2023
Accepted: December 12, 2023
Published: January 4, 2024

mixing, separating, and diagnosing blood and drug delivery in the blood.[5] Understanding and manipulating these driving forces are crucial for optimizing the performance of a LOC system. Such knowledge presents the opportunity to achieve higher efficiency and reliability in addressing cellular level challenges in medical diagnostics, forensic studies, cancer detection, and other fundamental research areas, for applications of point-of-care (POC) devices.[6]

1.2. Engineering Approach of Microfluidic Transport Phenomena in LOC Systems. Different transport mechanisms exhibit unique properties at submillimeter length scales in microfluidic devices, leading to significant transport phenomena that differ from those of macroscale flows. An in-depth understanding of these unique transport phenomena under microfluidic systems is often required in fluidic mechanics to fully harness the potential functionality of a LOC system to obtain systematically designed and precisely controlled transport of microfluids under their respective driving force. Fluid mechanics is considered a vital component in chemical engineering, enabling the analysis of fluid behaviors in various unit designs, ranging from large-scale reactors to separation units. Transport phenomena in fluid mechanics provide a conceptual framework for analytically and descriptively explaining why and how experimental results and physiological phenomena occur. The Navier−Stokes (N−S) equation, along with other governing equations, is often adapted to accurately describe fluid dynamics by accounting for pressure, surface properties, velocity, and temperature variations over space and time. In addition, limiting factors and nonidealities for these governing equations should be considered to impose corrections for empirical consistency before physical models are assembled for more accurate controls and efficiency. Microfluidic flow systems often deviate from ideal conditions, requiring adjustments to the standard governing equations. These deviations could arise from factors such as viscous effects, surface interactions, and non-Newtonian fluid properties from different microfluid types and geometrical layouts of microchannels. Addressing these nonidealities supports the refining of theoretical models and prediction accuracy for microfluidic flow behaviors.

The analytical calculation of coupled nonlinear governing equations, which describes the material and energy balances of systems under ideal conditions, often requires considerable computational efforts. However, advancements in computation capabilities, cost reduction, and improved accuracy have made numerical simulations using different numerical and modeling methods a powerful tool for effectively solving these complex coupled equations and modeling various transport phenomena. Computational fluid dynamics (CFD) is a numerical technique used to investigate the spatial and temporal distribution of various flow parameters. It serves as a critical approach to provide insights and reasoning for decision-making regarding the optimal designs involving fluid dynamics, even prior to complex physical model prototyping and experimental procedures. The integration of experimental data, theoretical analysis, and reliable numerical simulations from CFD enables systematic variation of analytical parameters through quantitative analysis, where adjustment to delivery of blood flow and other working fluids in LOC systems can be achieved.

Numerical methods such as the Finite-Difference Method (FDM), Finite-Element-Method (FEM), and Finite-Volume Method (FVM) are heavily employed in CFD and offer diverse approaches to achieve discretization of Eulerian flow equations through filling a mesh of the flow domain. A more in-depth review of numerical methods in CFD and its application for blood flow simulation is provided in Section 2.2.2.

1.3. Scope of the Review. In this Review, we explore and characterize the blood flow phenomena within the LOC systems, utilizing both physiological and engineering modeling approaches. Similar approaches will be taken to discuss capillary-driven flow and electric-osmotic flow (EOF) under electrokinetic phenomena as a passive and active transport scheme, respectively, for blood transport in LOC systems. Such an analysis aims to bridge the gap between physical (experimental) and engineering (analytical) perspectives in studying and manipulating blood flow delivery by different driving forces in LOC systems. Moreover, the Review hopes to benefit the interests of not only blood flow control in LOC devices but also the transport of viscoelastic fluids, which are less studied in the literature compared to that of Newtonian fluids, in LOC systems.

Section 2 examines the complex interplay between viscoelastic properties of blood and blood flow patterns under shear flow in LOC systems, while engineering numerical modeling approaches for blood flow are presented for assistance. Sections 3 and 4 look into the theoretical principles, numerical governing equations, and modeling methodologies for capillary driven flow and EOF in LOC systems as well as their impact on blood flow dynamics through the quantification of key parameters of the two driving forces. Section 5 concludes the characterized blood flow transport processes in LOC systems under these two forces. Additionally, prospective areas of research in improving the functionality of LOC devices employing blood and other viscoelastic fluids and potentially justifying mechanisms underlying microfluidic flow patterns outside of LOC systems are presented. Finally, the challenges encountered in the numerical studies of blood flow under LOC systems are acknowledged, paving the way for further research.

2. BLOOD FLOW PHENOMENA

2.1. Physiological Blood Flow Behavior. Blood, an essential physiological fluid in the human body, serves the vital role of transporting oxygen and nutrients throughout the body. Additionally, blood is responsible for suspending various blood cells including erythrocytes (red blood cells or RBCs), leukocytes (white blood cells), and thrombocytes (blood platelets) in a plasma medium.

Among the cells mentioned above, red blood cells (RBCs) comprise approximately 40−45% of the volume of healthy blood.[7] An RBC possesses an inherent elastic property with a biconcave shape of an average diameter of 8 μm and a thickness of 2 μm. This biconcave shape maximizes the surface-to-volume ratio, allowing RBCs to endure significant distortion while maintaining their functionality.[8,9] Additionally, the biconcave shape optimizes gas exchange, facilitating efficient uptake of oxygen due to the increased surface area. The inherent elasticity of RBCs allows them to undergo substantial distortion from their original biconcave shape and exhibits high flexibility, particularly in narrow channels.

RBC deformability enables the cell to deform from a biconcave shape to a parachute-like configuration, despite minor differences in RBC shape dynamics under shear flow between initial cell locations. As shown in Figure 1(a), RBCs initiating with different resting shapes and orientations displaying display a similar deformation pattern[10] in terms of its shape. Shear flow induces an inward bending of the cell at

https://doi.org/10.1021/cbe.3c00014
Chem Bio Eng. 2024, 1, 26−43

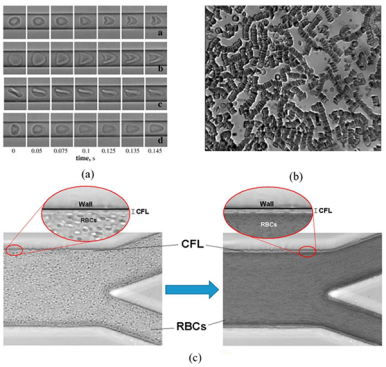

Figure 1. Images of varying deformation of RBCs and different dynamic blood flow behaviors. (a) The deforming shape behavior of RBCs at four different initiating positions under the same experimental conditions of a flow from left to right,[10] (b) RBC aggregation,[13] (c) CFL region.[18] Reproduced with permission from ref 10. Copyright 2011 Elsevier. Reproduced with permission from ref 13. Copyright 2022 The Authors, under the terms of the Creative Commons (CC BY 4.0) License https://creativecommons.org/licenses/by/4.0/. Reproduced with permission from ref 18. Copyright 2019 Elsevier.

the rear position of the rim to the final bending position,[11] resulting in an alignment toward the same position of the flow direction.

The flexible property of RBCs enables them to navigate through narrow capillaries and traverse a complex network of blood vessels. The deformability of RBCs depends on various factors, including the channel geometry, RBC concentration, and the elastic properties of the RBC membrane.[12] Both flexibility and deformability are vital in the process of oxygen exchange among blood and tissues throughout the body, allowing cells to flow in vessels even smaller than the original cell size prior to deforming.

As RBCs serve as major components in blood, their collective dynamics also hugely affect blood rheology. RBCs exhibit an aggregation phenomenon due to cell to cell interactions, such as adhesion forces, among populated cells, inducing unique blood flow patterns and rheological behaviors in microfluidic systems. For blood flow in large vessels between a diameter of 1 and 3 cm, where shear rates are not high, a constant viscosity and Newtonian behavior for blood can be assumed. However, under low shear rate conditions (0.1 s^{-1}) in smaller vessels such as the arteries and venules, which are within a diameter of 0.2 mm to 1 cm, blood exhibits non-Newtonian properties, such as shear-thinning viscosity and viscoelasticity due to RBC aggregation and deformability. The nonlinear viscoelastic property of blood gives rise to a complex relationship between viscosity and shear rate, primarily influenced by the highly elastic behavior of RBCs. A wide range of research on the transient behavior of the RBC shape and aggregation characteristics under varied flow circumstances has been conducted, aiming to obtain a better understanding of the interaction between blood flow shear forces from confined flows.

For a better understanding of the unique blood flow structures and rheological behaviors in microfluidic systems, some blood flow patterns are introduced in the following section.

2.1.1. RBC Aggregation. RBC aggregation is a vital phenomenon to be considered when designing LOC devices due to its impact on the viscosity of the bulk flow. Under conditions of low shear rate, such as in stagnant or low flow rate regions, RBCs tend to aggregate, forming structures known as rouleaux, resembling stacks of coins as shown in Figure 1(b).[13] The aggregation of RBCs increases the viscosity at the aggregated region,[14] hence slowing down the overall blood flow. However, when exposed to high shear rates, RBC aggregates disaggregate. As shear rates continue to increase, RBCs tend to deform, elongating and aligning themselves with the direction of the flow.[15] Such a dynamic shift in behavior from the cells in response to the shear rate forms the basis of the viscoelastic properties observed in whole blood. In essence, the viscosity of the blood varies according to the shear rate conditions, which are related to the velocity gradient of the system. It is significant to take the intricate relationship between shear rate conditions and the change of blood viscosity due to RBC aggregation into account since various flow driving conditions may induce varied effects on the degree of aggregation.

2.1.2. Fåhræus-Lindqvist Effect. The Fåhræus−Lindqvist (FL) effect describes the gradual decrease in the apparent viscosity of blood as the channel diameter decreases.[16] This effect is attributed to the migration of RBCs toward the central region in the microchannel, where the flow rate is higher, due to the presence of higher pressure and asymmetric distribution of shear forces. This migration of RBCs, typically observed at blood vessels less than 0.3 mm, toward the higher flow rate region contributes to the change in blood viscosity, which becomes dependent on the channel size. Simultaneously, the increase of the RBC concentration in the central region of the microchannel results in the formation of a less viscous region close to the microchannel wall. This region called the Cell-Free Layer (CFL), is primarily composed of plasma.[17] The combination of the FL effect and the following CFL formation provides a unique phenomenon that is often utilized in passive and active plasma separation mechanisms, involving branched and constriction channels for various applications in plasma separation using microfluidic systems.

2.1.3. Cell-Free Layer Formation. In microfluidic blood flow, RBCs form aggregates at the microchannel core and result in a region that is mostly devoid of RBCs near the microchannel walls, as shown in Figure 1(c).[18] The region is known as the cell-free layer (CFL). The CFL region is often known to possess a lower viscosity compared to other regions within the blood flow due to the lower viscosity value of plasma when compared to that of the aggregated RBCs. Therefore, a thicker CFL region composed of plasma correlates to a reduced apparent whole blood viscosity.[19] A thicker CFL region is often established following the RBC aggregation at the microchannel core under conditions of decreasing the tube diameter. Apart from the dependence on the RBC concentration in the microchannel core, the CFL thickness is also affected by the volume concentration of RBCs, or hematocrit, in whole blood, as well as the deformability of RBCs. Given the influence CFL thickness has on blood flow rheological parameters such as blood flow rate, which is strongly dependent on whole blood viscosity, investigating CFL thickness under shear flow is crucial for LOC systems accounting for blood flow.

2.1.4. Plasma Skimming in Bifurcation Networks. The uneven arrangement of RBCs in bifurcating microchannels, commonly termed skimming bifurcation, arises from the axial migration of RBCs within flowing streams. This uneven

https://doi.org/10.1021/cbe.3c00014
Chem Bio Eng. 2024, 1, 26−43

Table 1. Comparison of Various Non-Newtonian Models for Blood Viscosity[24−26]

Model	Non-Newtonian Viscosity	Parameters
Power Law	$\mu(\dot{\gamma}) = k\cdot(\dot{\gamma})^{n-1}$ (2)	n = 0.61, k = 0.42
Carreau	$\mu(\dot{\gamma}) = \mu_\infty + \frac{\mu_0 - \mu_\infty}{1 + (\lambda\dot{\gamma})}m$ (3)	μ_0 = 0.056 Pa·s, μ_∞ = 0.00345 Pa·s, λ = 3.1736 s, m = 2.406, a = 0.254
Walburn−Schneck	$\mu = C_1 e^{C_2 H_t} e^{C_4}\frac{\mathrm{TPMA}}{H_t^{\,2}}\dot{\gamma}^{-C_3 H_t}$ (4)	C_1 = 0.000797 Pa·s, C_2 = 0.0608 Pa·s, C_3 = 0.00499, C_4 = 14.585 g^{-1}, TPMA = 25 g/L
Carreau−Yasuda	$\frac{\mu(\dot{\gamma}) - \mu_\infty}{\mu_0 - \mu_\infty} = 1 + [(\lambda\dot{\gamma})^a](n-1)/a$ (5)	μ_0 = 0.056 Pa·s, μ_∞ = 0.00345 Pa·s, λ = 1.902 s, n = 0.22, a = 1.25
Quemada	$\mu = \mu_p\left(1 - \frac{1}{2}\frac{k_0 + k_\infty\sqrt{\frac{\dot{\gamma}}{\dot{\gamma}_c}}}{1 + \sqrt{\frac{\dot{\gamma}}{\dot{\gamma}_c}}}H_t\right)^{-2}$ (6)	μ_p = 0.0012 Pa·s, k_∞ = 2.07, k_0 = 4.33, $\dot{\gamma}_c$ = 1.88 s^{-1}

distribution contributes to variations in viscosity across differing sizes of bifurcating channels but offers a stabilizing effect. Notably, higher flow rates in microchannels are associated with increased hematocrit levels, resulting in higher viscosity compared with those with lower flow rates. Parametric investigations on bifurcation angle,[20] thickness of the CFL,[21] and RBC dynamics, including aggregation and deformation,[22] may alter the varying viscosity of blood and its flow behavior within microchannels.

2.2. Modeling on Blood Flow Dynamics. *2.2.1. Blood Properties and Mathematical Models of Blood Rheology.* Under different shear rate conditions in blood flow, the elastic characteristics and dynamic changes of the RBC induce a complex velocity and stress relationship, resulting in the incompatibility of blood flow characterization through standard presumptions of constant viscosity used for Newtonian fluid flow. Blood flow is categorized as a viscoelastic non-Newtonian fluid flow where constitutive equations governing this type of flow take into consideration the nonlinear viscometric properties of blood. To mathematically characterize the evolving blood viscosity and the relationship between the elasticity of RBC and the shear blood flow, respectively, across space and time of the system, a stress tensor ($\boldsymbol{\tau}$) defined by constitutive models is often coupled in the Navier−Stokes equation to account for the collective impact of the constant dynamic viscosity ($\boldsymbol{\eta}$) and the elasticity from RBCs on blood flow.

The dynamic viscosity of blood is heavily dependent on the shear stress applied to the cell and various parameters from the blood such as hematocrit value, plasma viscosity, mechanical properties of the RBC membrane, and red blood cell aggregation rate. The apparent blood viscosity is considered convenient for the characterization of the relationship between the evolving blood viscosity and shear rate, which can be defined by Casson's law, as shown in eq 1.

$$\mu = \frac{\tau_0}{\dot{\gamma}} + 2\sqrt{\frac{\eta\tau_0}{\dot{\gamma}}} + \eta \quad (1)$$

where τ_0 is the yield stress−stress required to initiate blood flow motion, η is the Casson rheological constant, and $\dot{\gamma}$ is the shear rate. The value of Casson's law parameters under blood with normal hematocrit level can be defined as τ_0 = 0.0056 Pa and η = 0.0035 Pa·s.[23] With the known property of blood and Casson's law parameters, an approximation can be made to the dynamic viscosity under various flow condition domains. The Power Law model is often employed to characterize the dynamic viscosity in relation to the shear rate, since precise solutions exist for specific geometries and flow circumstances, acting as a fundamental standard for definition. The Carreau and Carreau−Yasuda models can be advantageous over the Power Law model due to their ability to evaluate the dynamic viscosity at low to zero shear rate conditions. However, none of the above-mentioned models consider the memory or other elastic behavior of blood and its RBCs. Some other commonly used mathematical models and their constants for the non-Newtonian viscosity property characterization of blood are listed in Table 1 below.[24−26]

The blood rheology is commonly known to be influenced by two key physiological factors, namely, the hematocrit value (H_t) and the fibrinogen concentration (c_f), with an average value of 42% and 0.252 gd·L^{-1}, respectively. Particularly in low shear conditions, the presence of varying fibrinogen concentrations affects the tendency for aggregation and rouleaux formation, while the occurrence of aggregation is contingent upon specific levels of hematocrit.[27] The study from Apostolidis et al.[28] modifies the Casson model through emphasizing its reliance on hematocrit and fibrinogen concentration parameter values, owing to the extensive knowledge of the two physiological blood parameters.

The viscoelastic response of blood is heavily dependent on the elasticity of the RBC, which is defined by the relationship between the deformation and stress relaxation from RBCs under a specific location of shear flow as a function of the velocity field. The stress tensor is usually characterized by constitutive equations such as the Upper-Convected Maxwell Model[29] and the Oldroyd-B model[30] to track the molecule effects under shear from different driving forces. The prominent non-Newtonian features, such as shear thinning and yield stress, have played a vital role in the characterization of blood rheology, particularly with respect to the evaluation of yield stress under low shear conditions. The nature of stress measurement in blood, typically on the order of 1 mPa, is challenging due to its low magnitude. The occurrence of the CFL complicates the measurement further due to the significant decrease in apparent viscosity near the wall over time and a consequential disparity in viscosity compared to the bulk region.

In addition to shear thinning viscosity and yield stress, the formation of aggregation (rouleaux) from RBCs under low shear rates also contributes to the viscoelasticity under transient flow[31] and thixotropy[32] of whole blood. Given the difficulty in evaluating viscoelastic behavior of blood under low

https://doi.org/10.1021/cbe.3c00014
Chem Bio Eng. 2024, 1, 26−43

strain magnitudes and limitations in generalized Newtonian models, the utilization of viscoelastic models is advocated to encompass elasticity and delineate non-shear components within the stress tensor. Extending from the Oldroyd-B model, Anand et al.[33] developed a viscoelastic model framework for adapting elasticity within blood samples and predicting non-shear stress components. However, to also address the thixotropic effects, the model developed by Horner et al.[34] serves as a more comprehensive approach than the viscoelastic model from Anand et al. Thixotropy[32] typically occurs from the structural change of the rouleaux, where low shear rate conditions induce rouleaux formation. Correspondingly, elasticity increases, while elasticity is more representative of the isolated RBCs, under high shear rate conditions. The model of Horner et al.[34] considers the contribution of rouleaux to shear stress, taking into account factors such as the characteristic time for Brownian aggregation, shear-induced aggregation, and shear-induced breakage. Subsequent advancements in the model from Horner et al. often revolve around refining the three aforementioned key terms for a more substantial characterization of rouleaux dynamics. Notably, this has led to the recently developed mHAWB model[35] and other model iterations to enhance the accuracy of elastic and viscoelastic contributions to blood rheology, including the recently improved model suggested by Armstrong et al.[36]

2.2.2. Numerical Methods (FDM, FEM, FVM). Numerical simulation has become increasingly more significant in analyzing the geometry, boundary layers of flow, and nonlinearity of hyperbolic viscoelastic flow constitutive equations. CFD is a powerful and efficient tool utilizing numerical methods to solve the governing hydrodynamic equations, such as the Navier−Stokes (N−S) equation, continuity equation, and energy conservation equation, for qualitative evaluation of fluid motion dynamics under different parameters. CFD overcomes the challenge of analytically solving nonlinear forms of differential equations by employing numerical methods such as the Finite-Difference Method (FDM), Finite-Element Method (FEM), and Finite-Volume Method (FVM) to discretize and solve the partial differential equations (PDEs), allowing for qualitative reproduction of transport phenomena and experimental observations. Different numerical methods are chosen to cope with various transport systems for optimization of the accuracy of the result and control of error during the discretization process.

FDM is a straightforward approach to discretizing PDEs, replacing the continuum representation of equations with a set of finite-difference equations, which is typically applied to structured grids for efficient implementation in CFD programs.[37] However, FDM is often limited to simple geometries such as rectangular or block-shaped geometries and struggles with curved boundaries. In contrast, FEM divides the fluid domain into small finite grids or elements, approximating PDEs through a local description of physics.[38] All elements contribute to a large, sparse matrix solver. However, FEM may not always provide accurate results for systems involving significant deformation and aggregation of particles like RBCs due to large distortion of grids.[39] FVM evaluates PDEs following the conservation laws and discretizes the selected flow domain into small but finite size control volumes, with each grid at the center of a finite volume.[40] The divergence theorem allows the conversion of volume integrals of PDEs with divergence terms into surface integrals of surface fluxes across cell boundaries. Due to its conservation property, FVM offers efficient outcomes when dealing with PDEs that embody mass, momentum, and energy conservation principles. Furthermore, widely accessible software packages like the OpenFOAM toolbox[41] include a viscoelastic solver, making it an attractive option for viscoelastic fluid flow modeling.[42]

2.2.3. Modeling Methods of Blood Flow Dynamics. The complexity in the blood flow simulation arises from deformability and aggregation that RBCs exhibit during their interaction with neighboring cells under different shear rate conditions induced by blood flow. Numerical models coupled with simulation programs have been applied as a groundbreaking method to predict such unique rheological behavior exhibited by RBCs and whole blood. The conventional approach of a single-phase flow simulation is often applied to blood flow simulations within large vessels possessing a moderate shear rate. However, such a method assumes the properties of plasma, RBCs and other cellular components to be evenly distributed as average density and viscosity in blood, resulting in the inability to simulate the mechanical dynamics, such as RBC aggregation under high-shear flow field, inherent in RBCs. To accurately describe the asymmetric distribution of RBC and blood flow, multiphase flow simulation, where numerical simulations of blood flows are often modeled as two immiscible phases, RBCs and blood plasma, is proposed. A common assumption is that RBCs exhibit non-Newtonian behavior while the plasma is treated as a continuous Newtonian phase.

Numerous multiphase numerical models have been proposed to simulate the influence of RBCs on blood flow dynamics by different assumptions. In large-scale simulations (above the millimeter range), continuum-based methods are wildly used due to their lower computational demands.[43] Eulerian multiphase flow simulations offer the solution of a set of conservation equations for each separate phase and couple the phases through common pressure and interphase exchange coefficients. Xu et al.[44] utilized the combined finite-discrete element method (FDEM) to replicate the dynamic behavior and distortion of RBCs subjected to fluidic forces, utilizing the Johnson−Kendall−Roberts model[45] to define the adhesive forces of cell-to-cell interactions. The iterative direct-forcing immersed boundary method (IBM) is commonly employed in simulations of the fluid−cell interface of blood. This method effectively captures the intricacies of the thin and flexible RBC membranes within various external flow fields.[46] The study by Xu et al.[44] also adopts this approach to bridge the fluid dynamics and RBC deformation through IBM. Yoon and You utilized the Maxwell model to define the viscosity of the RBC membrane.[47] It was discovered that the Maxwell model could represent the stress relaxation and unloading processes of the cell. Furthermore, the reduced flexibility of an RBC under particular situations such as infection is specified, which was unattainable by the Kelvin−Voigt model[48] when compared to the Maxwell model in the literature. The Yeoh hyperplastic material model was also adapted to predict the nonlinear elasticity property of RBCs with FEM employed to discretize the RBC membrane using shell-type elements. Gracka et al.[49] developed a numerical CFD model with a finite-volume parallel solver for multiphase blood flow simulation, where an updated Maxwell viscoelasticity model and a Discrete Phase Model are adopted. In the study, the adapted IBM, based on unstructured grids, simulates the flow behavior and shape change of the RBCs through fluid-structure coupling. It was found that the hybrid Euler−Lagrange (E−L) approach[50] for

https://doi.org/10.1021/cbe.3c00014
Chem Bio Eng. 2024, 1, 26−43

the development of the multiphase model offered better results in the simulated CFL region in the microchannels.

To study the dynamics of individual behaviors of RBCs and the consequent non-Newtonian blood flow, cell-shape-resolved computational models are often adapted. The use of the boundary integral method has become prevalent in minimizing computational expenses, particularly in the exclusive determination of fluid velocity on the surfaces of RBCs, incorporating the option of employing IBM or particle-based techniques. The cell-shaped-resolved method has enabled an examination of cell to cell interactions within complex ambient or pulsatile flow conditions[51] surrounding RBC membranes. Recently, Rydquist et al.[52] have looked to integrate statistical information from macroscale simulations to obtain a comprehensive overview of RBC behavior within the immediate proximity of the flow through introduction of respective models characterizing membrane shape definition, tension, bending stresses of RBC membranes.

At a macroscopic scale, continuum models have conventionally been adapted for assessing blood flow dynamics through the application of elasticity theory and fluid dynamics. However, particle-based methods are known for their simplicity and adaptability in modeling complex multiscale fluid structures. Meshless methods, such as the boundary element method (BEM), smoothed particle hydrodynamics (SPH), and dissipative particle dynamics (DPD), are often used in particle-based characterization of RBCs and the surrounding fluid. By representing the fluid as discrete particles, meshless methods provide insights into the status and movement of the multiphase fluid. These methods allow for the investigation of cellular structures and microscopic interactions that affect blood rheology. Non-confronting mesh methods like IBM can also be used to couple a fluid solver such as FEM, FVM, or the Lattice Boltzmann Method (LBM) through membrane representation of RBCs. In comparison to conventional CFD methods, LBM has been viewed as a favorable numerical approach for solving the N−S equations and the simulation of multiphase flows. LBM exhibits the notable advantage of being amenable to high-performance parallel computing environments due to its inherently local dynamics. In contrast to DPD and SPH where RBC membranes are modeled as physically interconnected particles, LBM employs the IBM to account for the deformation dynamics of RBCs[53,54] under shear flows in complex channel geometries.[54,55] However, it is essential to acknowledge that the utilization of LBM in simulating RBC flows often entails a significant computational overhead, being a primary challenge in this context. Krüger et al.[56] proposed utilizing LBM as a fluid solver, IBM to couple the fluid and FEM to compute the response of membranes to deformation under immersed fluids. This approach decouples the fluid and membranes but necessitates significant computational effort due to the requirements of both meshes and particles.

Despite the accuracy of current blood flow models, simulating complex conditions remains challenging because of the high computational load and cost. Balachandran Nair et al.[57] suggested a reduced order model of RBC under the framework of DEM, where the RBC is represented by overlapping constituent rigid spheres. The Morse potential force is adapted to account for the RBC aggregation exhibited by cell to cell interactions among RBCs at different distances. Based upon the IBM, the reduced-order RBC model is adapted to simulate blood flow transport for validation under both single and multiple RBCs with a resolved CFD-DEM solver.[58] In the resolved CFD-DEM model, particle sizes are larger than the grid size for a more accurate computation of the surrounding flow field. A continuous forcing approach is taken to describe the momentum source of the governing equation prior to discretization, which is different from a Direct Forcing Method (DFM).[59] As no body-conforming moving mesh is required, the continuous forcing approach offers lower complexity and reduced cost when compared to the DFM. Piquet et al.[60] highlighted the high complexity of the DFM due to its reliance on calculating an additional immersed boundary flux for the velocity field to ensure its divergence-free condition.

The fluid−structure interaction (FSI) method has been advocated to connect the dynamic interplay of RBC membranes and fluid plasma within blood flow such as the coupling of continuum−particle interactions. However, such methodology is generally adapted for anatomical configurations such as arteries[61,62] and capillaries,[63] where both the structural components and the fluid domain undergo substantial deformation due to the moving boundaries. Due to the scope of the Review being blood flow simulation within microchannels of LOC devices without deformable boundaries, the Review of the FSI method will not be further carried out.

In general, three numerical methods are broadly used: mesh-based, particle-based, and hybrid mesh−particle techniques, based on the spatial scale and the fundamental numerical approach, mesh-based methods tend to neglect the effects of individual particles, assuming a continuum and being efficient in terms of time and cost. However, the particle-based approach highlights more of the microscopic and mesoscopic level, where the influence of individual RBCs is considered. A review from Freund et al.[64] addressed the three numerical methodologies and their respective modeling approaches of RBC dynamics. Given the complex mechanics and the diverse levels of study concerning numerical simulations of blood and cellular flow, a broad spectrum of numerical methods for blood has been subjected to extensive review.[64−70] Ye at al.[65] offered an extensive review of the application of the DPD, SPH, and LBM for numerical simulations of RBC, while Rathnayaka et al.[67] conducted a review of the particle-based numerical modeling for liquid marbles through drawing parallels to the transport of RBCs in microchannels. A comparative analysis between conventional CFD methods and particle-based approaches for cellular and blood flow dynamic simulation can be found under the review by Arabghahestani et al.[66] Literature by Li et al.[68] and Beris et al.[69] offer an overview of both continuum-based models at micro/macroscales and multiscale particle-based models encompassing various length and temporal dimensions. Furthermore, these reviews deliberate upon the potential of coupling continuum-particle methods for blood plasma and RBC modeling. Arciero et al.[70] investigated various modeling approaches encompassing cellular interactions, such as cell to cell or plasma interactions and the individual cellular phases. A concise overview of the reviews is provided in Table 2 for reference.

3. CAPILLARY DRIVEN BLOOD FLOW IN LOC SYSTEMS

3.1. Capillary Driven Flow Phenomena. Capillary driven (CD) flow is a pivotal mechanism in passive microfluidic flow systems[9] such as the blood circulation

https://doi.org/10.1021/cbe.3c00014
Chem Bio Eng. 2024, 1, 26−43

Table 2. List of Reviews for Numerical Approaches Employed in Blood Flow Simulation

Reference	Numerical methods
Li et al. (2013)[68]	Continuum-based modeling (BIM), particle-based modeling (LBM, LB-FE, SPH, DPD)
Freund (2014)[64]	RBC dynamic modeling (continuum-based modeling, complementary discrete microstructure modeling), blood flow dynamic modeling (FDM, IBM, LBM, particle-mesh methods, coupled boundary integral and mesh-based methods, DPD)
Ye et al. (2016)[65]	DPD, SPH, LBM, coupled IBM-Smoothed DPD
Arciero et al. (2017)[70]	LBM, IBM, DPD, conventional CFD Methods (FDM, FVM, FEM)
Arabghahestani et al. (2019)[66]	Particle-based methods (LBM, DPD, direct simulation Monte Carlo, molecular dynamics), SPH, conventional CFD methods (FDM, FVM, FEM)
Beris et al. (2021)[69]	DPD, smoothed DPD, IBM, LBM, BIM
Rathnayaka (2022)[67]	SPH, CG, LBM

system and LOC systems.[71] CD flow is essentially the movement of a liquid to flow against drag forces, where the capillary effect exerts a force on the liquid at the borders, causing a liquid−air meniscus to flow despite gravity or other drag forces. A capillary pressure drops across the liquid−air interface with surface tension in the capillary radius and contact angle. The capillary effect depends heavily on the interaction between the different properties of surface materials. Different values of contact angles can be manipulated and obtained under varying levels of surface wettability treatments to manipulate the surface properties, resulting in different CD blood delivery rates for medical diagnostic device microchannels. CD flow techniques are appealing for many LOC devices, because they require no external energy. However, due to the passive property of liquid propulsion by capillary forces and the long-term instability of surface treatments on channel walls, the adaptability of CD flow in geometrically complex LOC devices may be limited.

3.2. Theoretical and Numerical Modeling of Capillary Driven Blood Flow. *3.2.1. Theoretical Basis and Assumptions of Microfluidic Flow.* The study of transport phenomena regarding either blood flow driven by capillary forces or externally applied forces under microfluid systems all demands a comprehensive recognition of the significant differences in flow dynamics between microscale and macroscale. The fundamental assumptions and principles behind fluid transport at the microscale are discussed in this section. Such a comprehension will lay the groundwork for the following analysis of the theoretical basis of capillary forces and their role in blood transport in LOC systems.

At the macroscale, fluid dynamics are often strongly influenced by gravity due to considerable fluid mass. However, the high surface to volume ratio at the microscale shifts the balance toward surface forces (e.g., surface tension and viscous forces), much larger than the inertial force. This difference gives rise to transport phenomena unique to microscale fluid transport, such as the prevalence of laminar flow due to a very low Reynolds number (generally lower than 1). Moreover, the fluid in a microfluidic system is often assumed to be incompressible due to the small flow velocity, indicating constant fluid density in both space and time.

Microfluidic flow behaviors are governed by the fundamental principles of mass and momentum conservation, which are encapsulated in the continuity equation and the Navier−Stokes (N−S) equation. The continuity equation describes the conservation of mass, while the N−S equation captures the spatial and temporal variations in velocity, pressure, and other physical parameters. Under the assumption of the negligible influence of gravity in microfluidic systems, the continuity equation and the Eulerian representation of the incompressible N−S equation can be expressed as follows:

$$\nabla\cdot\vec{\mathbf{u}} = 0 \tag{7}$$

$$-\nabla p + \mu\nabla^2\vec{\mathbf{u}} + \nabla\cdot\vec{\tau} - \vec{\mathbf{F}} = 0 \tag{8}$$

Here, p is the pressure, $\mathbf{u}$ is the fluid viscosity, $\vec{\tau}$ represents the stress tensor, and $\mathbf{F}$ is the body force exerted by external forces if present.

3.2.2. Theoretical Basis and Modeling of Capillary Force in LOC Systems. The capillary force is often the major driving force to manipulate and transport blood without an externally applied force in LOC systems. Forces induced by the capillary effect impact the free surface of fluids and are represented not directly in the Navier−Stokes equations but through the pressure boundary conditions of the pressure term p. For hydrophilic surfaces, the liquid generally induces a contact angle between 0° and 30°, encouraging the spread and attraction of fluid under a positive $\cos\theta$ condition. For this condition, the pressure drop becomes positive and generates a spontaneous flow forward. A hydrophobic solid surface repels the fluid, inducing minimal contact. Generally, hydrophobic solids exhibit a contact angle larger than 90°, inducing a negative value of $\cos\theta$. Such a value will result in a negative pressure drop and a flow in the opposite direction. The induced contact angle is often utilized to measure the wall exposure of various surface treatments on channel walls where different wettability gradients and surface tension effects for CD flows are established. Contact angles between different interfaces are obtainable through standard values or experimental methods for reference.[72]

For the characterization of the induced force by the capillary effect, the Young−Laplace (Y−L) equation[73] is widely employed. In the equation, the capillary is considered a pressure boundary condition between the two interphases. Through the Y−L equation, the capillary pressure force can be determined, and subsequently, the continuity and momentum balance equations can be solved to obtain the blood filling rate. Kim et al.[74] studied the effects of concentration and exposure time of a nonionic surfactant, Silwet L-77, on the performance of a polydimethylsiloxane (PDMS) microchannel in terms of plasma and blood self-separation. The study characterized the capillary pressure force by incorporating the Y−L equation and further evaluated the effects of the changing contact angle due to different levels of applied channel wall surface treatments. The expression of the Y−L equation utilized by Kim et al.[74] is as follows:

$$P = -\sigma\left(\frac{\cos\theta_b + \cos\theta_t}{h} + \frac{\cos\theta_l + \cos\theta_r}{w}\right) \tag{9}$$

where σ is the surface tension of the liquid and θ_b, θ_t, θ_l, and θ_r are the contact angle values between the liquid and the bottom, top, left, and right walls, respectively. A numerical simulation through Coventor software is performed to evaluate the dynamic changes in the filling rate within the microchannel. The simulation results for the blood filling rate in the microchannel are expressed at a specific time stamp, shown in Figure 2. The results portray an increasing instantaneous

https://doi.org/10.1021/cbe.3c00014
Chem Bio Eng. 2024, 1, 26−43

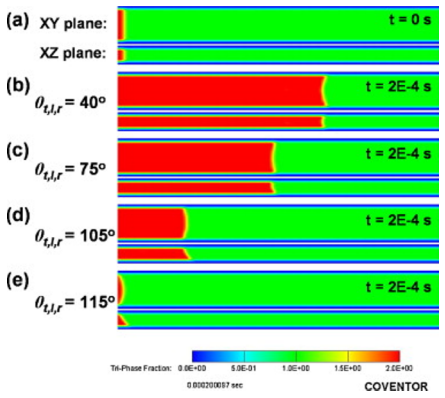

Figure 2. Numerical simulation of filling rate of capillary driven blood flow under various contact angle conditions at a specific timestamp.[74] Reproduced with permission from ref 74. Copyright 2010 Elsevier.

filling rate of blood in the microchannel following the decrease in contact angle induced by a higher concentration of the nonionic surfactant treated to the microchannel wall.

When in contact with hydrophilic or hydrophobic surfaces, blood forms a meniscus with a contact angle due to surface tension. The Lucas–Washburn (L–W) equation[75] is one of the pioneering theoretical definitions for the position of the meniscus over time. In addition, the L–W equation provides the possibility for research to obtain the velocity of the blood formed meniscus through the derivation of the meniscus position. The L–W equation[75] can be shown below:

$$L(t) = \sqrt{\frac{R\sigma \cos(\theta)t}{2\mu}} \tag{10}$$

Here $L(t)$ represents the distance of the liquid driven by the capillary forces. However, the generalized L–W equation solely assumes the constant physical properties from a Newtonian fluid rather than considering the non-Newtonian fluid behavior of blood. Cito et al.[76] constructed an enhanced version of the L–W equation incorporating the power law to consider the RBC aggregation and the FL effect. The non-Newtonian fluid apparent viscosity under the Power Law model is defined as

$$\mu = k\cdot(\dot{\gamma})^{n-1} \tag{11}$$

where $\dot{\gamma}$ is the strain rate tensor defined as $\dot{\gamma} = \sqrt{\frac{1}{2}\dot{\gamma}_{ij}\dot{\gamma}_{ji}}$. The stress tensor term $\boldsymbol{\tau}$ is computed as $\boldsymbol{\tau} = \mu\dot{\gamma}_{ij}$. The updated L–W equation by Cito[76] is expressed as

$$L(t) = R\left[\left(\frac{n+1}{3n+1}\right)\left(\frac{\sigma \cos(\theta)}{Rk}\right)^{1/n} t\right]^{n/n+1} \tag{12}$$

where k is the flow consistency index and n is the power law index, respectively. The power law index, from the Power Law model, characterizes the extent of the non-Newtonian behavior of blood. Both the consistency and power law index rely on blood properties such as hematocrit, the appearance of the FL effect, the formation of RBC aggregates, etc. The updated L–W equation computes the location and velocity of blood flow caused by capillary forces at specified time points within the LOC devices, taking into account the effects of blood flow characteristics such as RBC aggregation and the FL effect on dynamic blood viscosity.

Apart from the blood flow behaviors triggered by inherent blood properties, unique flow conditions driven by capillary forces that are portrayed under different microchannel geometries also hold crucial implications for CD blood delivery. Berthier et al.[77] studied the spontaneous Concus–Finn condition, the condition to initiate the spontaneous capillary flow within a V-groove microchannel, as shown in Figure 3(a) both experimentally and numerically. Through

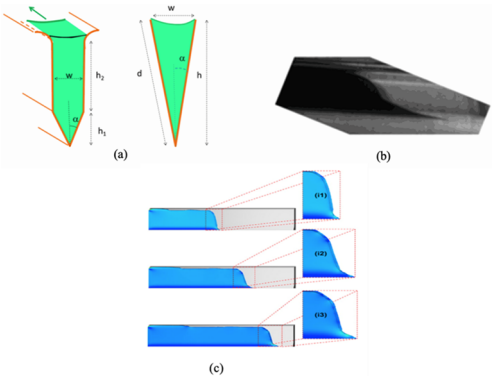

Figure 3. (a) Sketch of the cross-section of Berthier's V-groove microchannel, (b) experimental view of blood in the V-groove microchannel,[78] (c) illustration of the dynamic change of the extension of filament from FLOW 3D under capillary flow at three increasing time intervals.[78] Reproduced with permission from ref 78. Copyright 2014 Elsevier.

experimental studies, the spontaneous Concus–Finn filament development of capillary driven blood flow is observed, as shown in Figure 3(b), while the dynamic development of blood flow is numerically simulated through CFD simulation.

Berthier et al.[77] characterized the contact angle needed for the initiation of the capillary driving force at a zero-inlet pressure, through the half-angle (α) of the V-groove geometry layout, and its relation to the Concus–Finn filament as shown below:

$$\begin{cases} \theta < \dfrac{\pi}{2} - \alpha \\ \dfrac{\sin\alpha}{1 + 2(h_2/w)\sin\alpha} < \cos\theta \end{cases} \tag{13}$$

Three possible regimes were concluded based on the contact angle value for the initiation of flow and development of Concus–Finn filament:

$$\begin{cases} \theta > \theta_1 & \text{no SCF} \\ \theta_1 > \theta > \theta_0 & \text{SCF without a Concus–Finn filament} \\ \theta_0 & \text{SCF without a Concus–Finn filament} \end{cases} \tag{14}$$

Under Newton's Law, the force balance with low Reynolds and Capillary numbers results in the neglect of inertial terms. The force balance between the capillary forces and the viscous force induced by the channel wall is proposed to derive the analytical fluid velocity. This relation between the two forces offers insights into the average flow velocity and the penetration distance function dependent on time. The apparent blood viscosity is defined by Berthier et al.[78] through Casson's law,[23] given in eq 1. The research used the FLOW-3D program from

https://doi.org/10.1021/cbe.3c00014
Chem Bio Eng. 2024, 1, 26–43

Flow Science Inc. software, which solves transient, free-surface problems using the FDM in multiple dimensions. The Volume of Fluid (VOF) method[79] is utilized to locate and track the dynamic extension of filament throughout the advancing interface within the channel ahead of the main flow at three progressing time stamps, as depicted in Figure 3(c).

4. ELECTRO-OSMOTIC FLOW (EOF) IN LOC SYSTEMS

The utilization of external forces, such as electric fields, has significantly broadened the possibility of manipulating microfluidic flow in LOC systems.[80] Externally applied electric field forces induce a fluid flow from the movement of ions in fluid terms as the "electro-osmotic flow" (EOF).

Unique transport phenomena, such as enhanced flow velocity and flow instability, induced by non-Newtonian fluids, particularly viscoelastic fluids, under EOF, have sparked considerable interest in microfluidic devices with simple or complicated geometries within channels.[81] However, compared to the study of Newtonian fluids and even other electro-osmotic viscoelastic fluid flows, the literature focusing on the theoretical and numerical modeling of electro-osmotic blood flow is limited due to the complexity of blood properties. Consequently, to obtain a more comprehensive understanding of the complex blood flow behavior under EOF, theoretical and numerical studies of the transport phenomena in the EOF section will be based on the studies of different viscoelastic fluids under EOF rather than that of blood specifically. Despite this limitation, we believe these studies offer valuable insights that can help understand the complex behavior of blood flow under EOF.

4.1. EOF Phenomena. Electro-osmotic flow occurs at the interface between the microchannel wall and bulk phase solution. When in contact with the bulk phase, solution ions are absorbed or dissociated at the solid−liquid interface, resulting in the formation of a charge layer, as shown in Figure 4. This charged channel surface wall interacts with both

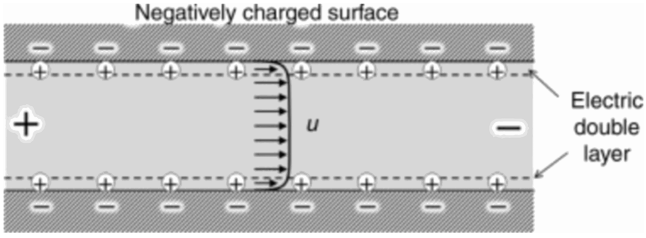

Figure 4. Schematic diagram of an electro-osmotic flow in a microchannel with negative surface charge.[82] Reproduced with permission from ref 82. Copyright 2012 Woodhead Publishing.

negative and positive ions in the bulk sample, causing repulsion and attraction forces to create a thin layer of immobilized counterions, known as the Stern layer. The induced electric potential from the wall gradually decreases with an increase in the distance from the wall. The Stern layer potential, commonly termed the zeta potential, controls the intensity of the electrostatic interactions between mobile counterions and, consequently, the drag force from the applied electric field. Next to the Stern layer is the diffuse mobile layer, mainly composed of a mobile counterion. These two layers constitute the "electrical double layer" (EDL), the thickness of which is directly proportional to the ionic strength (concentration) of the bulk fluid. The relationship between the two parameters is characterized by a Debye length (λ_D), expressed as

$$\lambda_D = \sqrt{\frac{\epsilon k_B T}{2(Ze)^2 c_0}} \tag{15}$$

where ϵ is the permittivity of the electrolyte solution, k_B is the Boltzmann constant, T is the electron temperature, Z is the integer valence number, e is the elementary charge, and c_0 is the ionic density.

When an electric field is applied perpendicular to the EDL, viscous drag is generated due to the movement of excess ions in the EDL. Electro-osmotic forces can be attributed to the externally applied electric potential ($\boldsymbol{\phi}$) and the zeta potential, the system wall induced potential by charged walls ($\boldsymbol{\psi}$). As illustrated in Figure 4, the majority of ions in the bulk phase have a uniform velocity profile, except for a shear rate condition confined within an extremely thin Stern layer. Therefore, EOF displays a unique characteristic of a "near flat" or plug flow velocity profile, different from the parabolic flow typically induced by pressure-driven microfluidic flow (Hagen−Poiseuille flow). The plug-shaped velocity profile of the EOF possesses a high shear rate above the Stern layer.

Overall, the EOF velocity magnitude is typically proportional to the Debye Length (λ_D), zeta potential, and magnitude of the externally applied electric field, while a more viscous liquid reduces the EOF velocity.

4.2. Modeling on Electro-osmotic Viscoelastic Fluid Flow. *4.2.1. Theoretical Basis of EOF Mechanisms.* The EOF of an incompressible viscoelastic fluid is commonly governed by the continuity and incompressible N−S equations, as shown in eqs 7 and 8, where the stress tensor and the electrostatic force term are coupled. The electro-osmotic body force term **F**, representing the body force exerted by the externally applied electric force, is defined as $\vec{F} = p_E\vec{E}$, where ρ_E and $\vec{E}$ are the net electric charge density and the applied external electric field, respectively.

Numerous models are established to theoretically study the externally applied electric potential and the system wall induced potential by charged walls. The following Laplace equation, expressed as eq 16, is generally adapted and solved to calculate the externally applied potential ($\boldsymbol{\phi}$).

$$\nabla^2\phi = 0 \tag{16}$$

Ion diffusion under applied electric fields, together with mass transport resulting from convection and diffusion, transports ionic solutions in bulk flow under electrokinetic processes. The Nernst−Planck equation can describe these transport methods, including convection, diffusion, and electro-diffusion. Therefore, the Nernst−Planck equation is used to determine the distribution of the ions within the electrolyte. The electric potential induced by the charged channel walls follows the Poisson−Nernst−Plank (PNP) equation, which can be written as eq 17.

$$\nabla\cdot\left[D_i\nabla n_i - \vec{u}n_i + \frac{n_i D_i z_i e}{k_b T}\nabla(\phi + \psi)\right] = 0 \tag{17}$$

where D_i, n_i, and z_i are the diffusion coefficient, ionic concentration, and ionic valence of the ionic species I, respectively. However, due to the high nonlinearity and numerical stiffness introduced by different lengths and time scales from the PNP equations, the Poisson−Boltzmann (PB)

https://doi.org/10.1021/cbe.3c00014
Chem Bio Eng. 2024, 1, 26−43

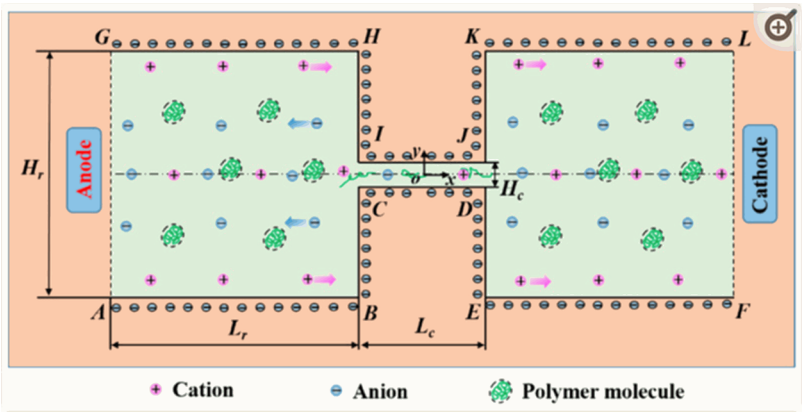

Figure 5. Schematic diagram of a negatively charged constriction microchannel connected to two reservoirs at both ends. An electro-osmotic flow is induced in the system by the induced potential difference between the anode and cathode.[90] Reproduced with permission from ref 90. Copyright 2021 The Authors, under the terms of the Creative Commons (CC BY 4.0) License https://creativecommons.org/licenses/by/4.0/.

model is often considered the major simplified method of the PNP equation to characterize the potential distribution of the EDL region in microchannels. In the PB model, it is assumed that the ionic species in the fluid follow the Boltzmann distribution. This model is typically valid for steady-state problems where charge transport can be considered negligible, the EDLs do not overlap with each other, and the intrinsic potentials are low. It provides a simplified representation of the potential distribution in the EDL region. The PB equation governing the EDL electric potential distribution is described as

$$\nabla^2\psi = \left(\frac{2ezn_0}{\varepsilon\varepsilon_0}\right)\sinh\left(\frac{ze\psi}{k_bT}\right) \tag{18}$$

where n_0 is the ion bulk concentration, z is the ionic valence, and ε_0 is the electric permittivity in the vacuum. Under low electric potential conditions, an even further simplified model to illustrate the EOF phenomena is the Debye−Hückel (DH) model. The DH model is derived by obtaining a charge density term by expanding the exponential term of the Boltzmann equation in a Taylor series.

4.2.2. EOF Modeling for Viscoelastic Fluids. Many studies through numerical modeling were performed to obtain a deeper understanding of the effect exhibited by externally applied electric fields on viscoelastic flow in microchannels under various geometrical designs. Bello et al.[83] found that methylcellulose solution, a non-Newtonian polymer solution, resulted in stronger electro-osmotic mobility in experiments when compared to the predictions by the Helmholtz−Smoluchowski equation, which is commonly used to define the velocity of EOF of a Newtonian fluid. Being one of the pioneers to identify the discrepancies between the EOF of Newtonian and non-Newtonian fluids, Bello et al. attributed such discrepancies to the presence of a very high shear rate in the EDL, resulting in a change in the orientation of the polymer molecules. Park and Lee[84] utilized the FVM to solve the PB equation for the characterization of the electric field induced force. In the study, the concept of fractional calculus for the Oldroyd-B model was adapted to illustrate the elastic and memory effects of viscoelastic fluids in a straight microchannel They observed that fluid elasticity and increased ratio of viscoelastic fluid contribution to overall fluid viscosity had a significant impact on the volumetric flow rate and sensitivity of velocity to electric field strength compared to Newtonian fluids. Afonso et al.[85] derived an analytical expression for EOF of viscoelastic fluid between parallel plates using the DH model to account for a zeta potential condition below 25 mV. The study established the understanding of the electro-osmotic viscoelastic fluid flow under low zeta potential conditions. Apart from the electrokinetic forces, pressure forces can also be coupled with EOF to generate a unique fluid flow behavior within the microchannel. Sousa et al.[86] analytically studied the flow of a standard viscoelastic solution by combining the pressure gradient force with an externally applied electric force. It was found that, at a near wall skimming layer and the outer layer away from the wall, macromolecules migrating away from surface walls in viscoelastic fluids are observed. In the study, the Phan-Thien Tanner (PTT) constitutive model is utilized to characterize the viscoelastic properties of the solution. The approach is found to be valid when the EDL is much thinner than the skimming layer under an enhanced flow rate. Zhao and Yang[87] solved the PB equation and Carreau model for the characterization of the EOF mechanism and non-Newtonian fluid respectively through the FEM. The numerical results depict that, different from the EOF of Newtonian fluids, non-Newtonian fluids led to an increase of electro-osmotic mobility for shear thinning fluids but the opposite for shear thickening fluids.

Like other fluid transport driving forces, EOF within unique geometrical layouts also portrays unique transport phenomena. Pimenta and Alves[88] utilized the FVM to perform numerical simulations of the EOF of viscoelastic fluids considering the PB equation and the Oldroyd-B model, in a cross-slot and flow-focusing microdevices. It was found that electroelastic instabilities are formed due to the development of large stresses inside the EDL with streamlined curvature at geometry corners. Bezerra et al.[89] used the FDM to numerically analyze the vortex formation and flow instability from an electro-osmotic non-Newtonian fluid flow in a microchannel with a nozzle geometry and parallel wall geometry setting. The PNP equation is utilized to characterize the charge motion in the EOF and the PTT model for non-Newtonian flow characterization. A constriction geometry is commonly utilized in blood flow adapted in LOC systems due to the change in blood flow behavior under narrow dimensions in a microchannel. Ji et al.[90] recently studied the EOF of viscoelastic fluid in a constriction microchannel connected by two relatively big reservoirs on

https://doi.org/10.1021/cbe.3c00014
Chem Bio Eng. 2024, 1, 26−43

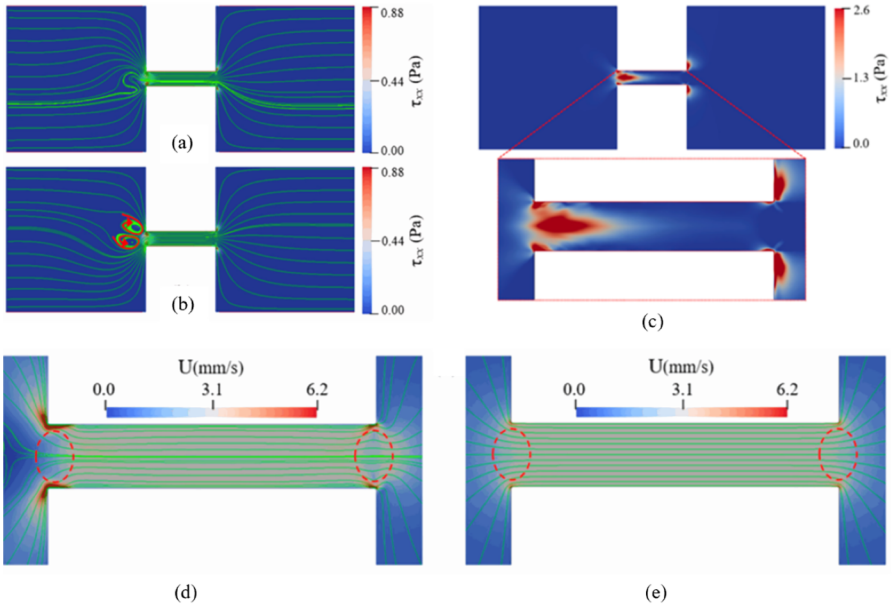

Figure 6. Schematic diagram of vortex formation and streamlines of EOF depicting flow instability at (a) 1.71 s and (b) 1.75 s. Spatial distribution of the elastic normal stress at (c) high E_{app} condition. Streamline of an electro-osmotic flow under E_{app} of 600 V/cm[90] for (d) non-Newtonian and (e) Newtonian fluid through a constriction geometry. Reproduced with permission from ref 90. Copyright 2021 The Authors, under the terms of the Creative Commons (CC BY 4.0) License https://creativecommons.org/licenses/by/4.0/.

both ends (as seen in Figure 5) filled with the polyacrylamide polymer solution, a viscoelastic fluid, and an incompressible monovalent binary electrolyte solution KCl.

In studying the EOF of viscoelastic fluids, the Oldroyd-B model is often utilized to characterize the polymeric stress tensor and the deformation rate of the fluid. The Oldroyd-B model is expressed as follows:

$$\tau = \frac{\eta_p}{\lambda}(\mathbf{c} - \mathbf{I}) \tag{19}$$

where η_p, λ, $\mathbf{c}$, and $\mathbf{I}$ represent the polymer dynamic viscosity, polymer relaxation time, symmetric conformation tensor of the polymer molecules, and the identity matrix, respectively.

A log-conformation tensor approach is taken to prevent convergence difficulty induced by the viscoelastic properties. The conformation tensor ($\mathbf{c}$) in the polymeric stress tensor term is redefined by a new tensor ($\boldsymbol{\Theta}$) based on the natural logarithm of the $\mathbf{c}$. The new tensor is defined as

$$\Theta = \ln(\mathbf{c}) = \mathbf{R}\ln(\boldsymbol{\Lambda})\mathbf{R} \tag{20}$$

in which $\boldsymbol{\Lambda}$ is the diagonal matrix and $\mathbf{R}$ is the orthogonal matrix.

Under the new conformation tensor, the induced EOF of a viscoelastic fluid is governed by the continuity and N−S equations adapting the Oldroyd-B model, which is expressed as

$$\frac{\partial \boldsymbol{\Theta}}{\partial t} + \mathbf{u}\cdot\nabla\boldsymbol{\Theta} = \boldsymbol{\Omega}\Theta - \Theta\boldsymbol{\Omega} + 2\mathbf{B} + \frac{1}{\lambda}(e^{\Theta} - \mathbf{I}) \tag{21}$$

where $\boldsymbol{\Omega}$ and $\mathbf{B}$ represent the anti-symmetric matrix and the symmetric traceless matrix of the decomposition of the velocity gradient tensor $\nabla\mathbf{u}$, respectively. The conformation tensor can be recovered by $\mathbf{c} = \exp(\Theta)$. The PB model and Laplace equation are utilized to characterize the charged channel wall induced potential and the externally applied potential.

The governing equations are numerically solved through the FVM by RheoTool,[42] an open-source viscoelastic EOF solver on the OpenFOAM platform. A SIMPLEC (Semi-Implicit Method for Pressure Linked Equations-Consistent) algorithm was applied to solve the velocity-pressure coupling. The pressure field and velocity field were computed by the PCG (Preconditioned Conjugate Gradient) solver and the PBiCG (Preconditioned Biconjugate Gradient) solver, respectively.

Ranging magnitudes of an applied electric field or fluid concentration induce both different streamlines and velocity magnitudes at various locations and times of the microchannel. In the study performed by Ji et al.,[90] notable fluctuation of streamlines and vortex formation is formed at the upper stream entrance of the constriction as shown in Figure 6(a) and (b), respectively, due to the increase of electrokinetic effect, which is seen as a result of the increase in polymeric stress (τ_{xx}).[90] The contraction geometry enhances the EOF velocity within the constriction channel under high E_{app} condition (600 V/cm). Such phenomena can be attributed to the dependence of electro-osmotic viscoelastic fluid flow on the system wall surface and bulk fluid properties.[91]

As elastic normal stress exceeds the local shear stress, flow instability and vortex formation occur. The induced elastic stress under EOF not only enhances the instability of the flow but often generates an irregular secondary flow leading to strong disturbance.[92] It is also vital to consider the effect of the constriction layout of microchannels on the alteration of the field strength within the system. The contraction geometry enhances a larger electric field strength compared with other locations of the channel outside the constriction region, resulting in a higher velocity gradient and stronger extension on the polymer within the viscoelastic solution. Following the high shear flow condition, a higher magnitude of stretch for polymer molecules in viscoelastic fluids exhibits larger elastic stresses and enhancement of vortex formation at the region.[93]

As shown in Figure 6(c), significant elastic normal stress occurs at the inlet of the constriction microchannel. Such occurrence of a polymeric flow can be attributed to the dominating elongational flow, giving rise to high deformation

https://doi.org/10.1021/cbe.3c00014
Chem Bio Eng. 2024, 1, 26−43

of the polymers within the viscoelastic fluid flow, resulting in higher elastic stress from the polymers. Such phenomena at the entrance result in the difference in velocity streamline as circled in Figure 6(d) compared to that of the Newtonian fluid at the constriction entrance in Figure 6(e).[90] The difference between the Newtonian and polymer solution at the exit, as circled in Figure 6(d) and (e), can be attributed to the extrudate swell effect of polymers[94] within the viscoelastic fluid flow. The extrudate swell effect illustrates that, as polymers emerge from the constriction exit, they tend to contract in the flow direction and grow in the normal direction, resulting in an extrudate diameter greater than the channel size. The deformation of polymers within the polymeric flow at both the entrance and exit of the contraction channel facilitates the change in shear stress conditions of the flow, leading to the alteration in streamlines of flows for each region.

4.3. EOF Applications in LOC Systems. *4.3.1. Mixing in LOC Systems.* Rather than relying on the micromixing controlled by molecular diffusion under low Reynolds number conditions, active mixers actively leverage convective instability and vortex formation induced by electro-osmotic flows from alternating current (AC) or direct current (DC) electric fields. Such adaptation is recognized as significant breakthroughs for promotion of fluid mixing in chemical and biological applications such as drug delivery, medical diagnostics, chemical synthesis, and so on.[95]

Many researchers proposed novel designs of electro-osmosis micromixers coupled with numerical simulations in conjunction with experimental findings to increase their understanding of the role of flow instability and vortex formation in the mixing process under electrokinetic phenomena. Matsubara and Narumi[96] numerically modeled the mixing process in a microchannel with four electrodes on each side of the microchannel wall, which generated a disruption through unstable electro-osmotic vortices. It was found that particle mixing was sensitive to both the convection effect induced by the main and secondary vortex within the micromixer and the change in oscillation frequency caused by the supplied AC voltage when the Reynolds number was varied. Qaderi et al.[97] adapted the PNP equation to numerically study the effect of the geometry and zeta potential configuration of the microchannel on the mixing process with a combined electro-osmotic pressure driven flow. It was reported that the application of heterogeneous zeta potential configuration enhances the mixing efficiency by around 23% while the height of the hurdles increases the mixing efficiency at most 48.1%. Cho et al.[98] utilized the PB model and Laplace equation to numerically simulate the electro-osmotic non-Newtonian fluid mixing process within a wavy and block layout of microchannel walls. The Power Law model is adapted to describe the fluid rheological characteristic. It was found that shear-thinning fluids possess a higher volumetric flow rate, which could result in poorer mixing efficiency compared to that of Newtonian fluids. Numerous studies have revealed that flow instability and vortex generation, in particular secondary vortices produced by barriers or greater magnitudes of heterogeneous zeta potential distribution, enhance mixing by increasing bulk flow velocity and reducing flow distance.

To better understand the mechanism of disturbance formed in the system due to externally applied forces, known as electrokinetic instability, literature often utilize the Rayleigh (Ra) number,[1] as described below:

$$Ra_v = \frac{u_{ev}}{u_{eo}} = \left(\frac{\gamma - 1}{\gamma + 1}\right)^2 \frac{W}{\delta} \frac{2E_{el}{}^2 H^2}{\zeta\delta} \tag{22}$$

where γ is the conductivity ratio of the two streams and can be written as $\gamma = \frac{\sigma_{el,H}}{\sigma_{el,L}}$. The Ra number characterizes the ratio between electroviscous and electro-osmotic flow. A high Ra_v value often results in good mixing. It is evident that fluid properties such as the conductivity (σ) of the two streams play a key role in the formation of disturbances to enhance mixing in microsystems. At the same time, electrokinetic parameters like the zeta potential (ζ) in the Ra number is critical in the characterization of electro-osmotic velocity and a slip boundary condition at the microchannel wall.

To understand the mixing result along the channel, the concentration field can be defined and simulated under the assumption of steady state conditions and constant diffusion coefficient for each of the working fluid within the system through the convection−diffusion equation as below:

$$\frac{\partial c_i}{\partial t} + \vec{\nabla}(c_i\vec{u} - D_i\vec{\nabla}c_i) = 0 \tag{23}$$

where c_i is the species concentration of species i and D_i is the diffusion coefficient of the corresponding species.

The standard deviation of concentration (σ_{sd}) can be adapted to evaluate the mixing quality of the system.[97] The standard deviation for concentration at a specific portion of the channel may be calculated using the equation below:

$$\sigma_{sd} = \sqrt{\frac{\int_0^1 (C^*(y^*) - C_m)^2 \, dy^*}{\int_0^1 dy^*}} \tag{24}$$

where $C^*(y^*)$ and C_m are the non-dimensional concentration profile and the mean concentration at the portion, respectively. C^* is the non-dimensional concentration and can be calculated as $C^* = \frac{C}{C_{ref}}$, where C_{ref} is the reference concentration defined as the bulk solution concentration. The mean concentration profile can be calculated as $C_m = \frac{\int_0^1 (C^*(y^*)\, dy^*}{\int_0^1 dy^*}$. With the standard deviation of concentration, the mixing efficiency[97] can then be calculated as below:

$$\varepsilon_x = 1 - \frac{\sigma_{sd}}{\sigma_{sd,0}} \tag{25}$$

where $\sigma_{sd,0}$ is the standard derivation of the case of no mixing. The value of the mixing efficiency is typically utilized in conjunction with the simulated flow field and concentration field to explore the effect of geometrical and electrokinetic parameters on the optimization of the mixing results.

5. SUMMARY

5.1. Conclusion. Viscoelastic fluids such as blood flow in LOC systems are an essential topic to proceed with diagnostic analysis and research through microdevices in the biomedical and pharmaceutical industries. The complex blood flow behavior is tightly controlled by the viscoelastic characteristics of blood such as the dynamic viscosity and the elastic property of RBCs under various shear rate conditions. Furthermore, the flow behaviors under varied driving forces promote an array of microfluidic transport phenomena that are critical to the

https://doi.org/10.1021/cbe.3c00014
Chem Bio Eng. 2024, 1, 26−43

management of blood flow and other adapted viscoelastic fluids in LOC systems. This review addressed the blood flow phenomena, the complicated interplay between shear rate and blood flow behaviors, and their numerical modeling under LOC systems through the lens of the viscoelasticity characteristic. Furthermore, a theoretical understanding of capillary forces and externally applied electric forces leads to an in-depth investigation of the relationship between blood flow patterns and the key parameters of the two driving forces, the latter of which is introduced through the lens of viscoelastic fluids, coupling numerical modeling to improve the knowledge of blood flow manipulation in LOC systems. The flow disturbances triggered by the EOF of viscoelastic fluids and their impact on blood flow patterns have been deeply investigated due to their important role and applications in LOC devices. Continuous advancements of various numerical modeling methods with experimental findings through more efficient and less computationally heavy methods have served as an encouraging sign of establishing more accurate illustrations of the mechanisms for multiphase blood and other viscoelastic fluid flow transport phenomena driven by various forces. Such progress is fundamental for the manipulation of unique transport phenomena, such as the generated disturbances, to optimize functionalities offered by microdevices in LOC systems.

The following section will provide further insights into the employment of studied blood transport phenomena to improve the functionality of micro devices adapting LOC technology. A discussion of the novel roles that external driving forces play in microfluidic flow behaviors is also provided. Limitations in the computational modeling of blood flow and electrokinetic phenomena in LOC systems will also be emphasized, which may provide valuable insights for future research endeavors. These discussions aim to provide guidance and opportunities for new paths in the ongoing development of LOC devices that adapt blood flow.

5.2. Future Directions. *5.2.1. Electro-osmosis Mixing in LOC Systems.* Despite substantial research, mixing results through flow instability and vortex formation phenomena induced by electro-osmotic mixing still deviate from the effective mixing results offered by chaotic mixing results such as those seen in turbulent flows. However, recent discoveries of a mixing phenomenon that is generally observed under turbulent flows are found within electro-osmosis micromixers under low Reynolds number conditions. Zhao[99] experimentally discovered a rapid mixing process in an AC applied micromixer, where the power spectrum of concentration under an applied voltage of 20 $V_{p\text{-}p}$ induces a $-5/3$ slope within a frequency range. This value of the slope is considered as the O−C spectrum in macroflows, which is often visible under relatively high *Re* conditions, such as the Taylor microscale Reynolds number $Re > 500$ in turbulent flows.[100] However, the *Re* value in the studied system is less than 1 at the specific location and applied voltage. A secondary flow is also suggested to occur close to microchannel walls, being attributed to the increase of convective instability within the system.

Despite the experimental phenomenon proposed by Zhao et al.,[99] the range of effects induced by vital parameters of an EOF mixing system on the enhanced mixing results and mechanisms of disturbance generated by the turbulent-like flow instability is not further characterized. Such a gap in knowledge may hinder the adaptability and commercialization of the discovery of micromixers. One of the parameters for further evaluation is the conductivity gradient of the fluid flow. A relatively strong conductivity gradient (5000:1) was adopted in the system due to the conductive properties of the two fluids. The high conductivity gradients may contribute to the relatively large Rayleigh number and differences in EDL layer thickness, resulting in an unusual disturbance in laminar flow conditions and enhanced mixing results. However, high conductivity gradients are not always achievable by the working fluids due to diverse fluid properties. The reliance on turbulent-like phenomena and rapid mixing results in a large conductivity gradient should be established to prevent the limited application of fluids for the mixing system. In addition, the proposed system utilizes distinct zeta potential distributions at the top and bottom walls due to their difference in material choices, which may be attributed to the flow instability phenomena. Further studies should be made on varying zeta potential magnitude and distribution to evaluate their effect on the slip boundary conditions of the flow and the large shear rate condition close to the channel wall of EOF. Such a study can potentially offer an optimized condition in zeta potential magnitude through material choices and geometrical layout of the zeta potential for better mixing results and manipulation of mixing fluid dynamics. The two vital parameters mentioned above can be varied with the aid of numerical simulation to understand the effect of parameters on the interaction between electro-osmotic forces and electro-viscous forces. At the same time, the relationship of developed streamlines of the simulated velocity and concentration field, following their relationship with the mixing results, under the impact of these key parameters can foster more insight into the range of impact that the two parameters have on the proposed phenomena and the microfluidic dynamic principles of disturbances.

In addition, many of the current investigations of electrokinetic mixers commonly emphasize the fluid dynamics of mixing for Newtonian fluids, while the utilization of biofluids, primarily viscoelastic fluids such as blood, and their distinctive response under shear forces in these novel mixing processes of LOC systems are significantly less studied. To develop more compatible microdevice designs and efficient mixing outcomes for the biomedical industry, it is necessary to fill the knowledge gaps in the literature on electro-osmotic mixing for biofluids, where properties of elasticity, dynamic viscosity, and intricate relationship with shear flow from the fluid are further considered.

5.2.2. Electro-osmosis Separation in LOC Systems. Particle separation in LOC devices, particularly in biological research and diagnostics, is another area where disturbances may play a significant role in optimization.[101] Plasma analysis in LOC systems under precise control of blood flow phenomena and blood/plasma separation procedures can detect vital information about infectious diseases from particular antibodies and foreign nucleic acids for medical treatments, diagnostics, and research,[102] offering more efficient results and simple operating procedures compared to that of the traditional centrifugation method for blood and plasma separation. However, the adaptability of LOC devices for blood and plasma separation is often hindered by microchannel clogging, where flow velocity and plasma yield from LOC devices is reduced due to occasional RBC migration and aggregation at the filtration entrance of microdevices.[103]

https://doi.org/10.1021/cbe.3c00014
Chem Bio Eng. 2024, 1, 26−43

It is important to note that the EOF induces flow instability close to microchannel walls, which may provide further solutions to clogging for the separation process of the LOC systems. Mohammadi et al.[104] offered an anti-clogging effect of RBCs at the blood and plasma separating device filtration entry, adjacent to the surface wall, through RBC disaggregation under high shear rate conditions generated by a forward and reverse EOF direction.

Further theoretical and numerical research can be conducted to characterize the effect of high shear rate conditions near microchannel walls toward the detachment of binding blood cells on surfaces and the reversibility of aggregation. Through numerical modeling with varying electrokinetic parameters to induce different degrees of disturbances or shear conditions at channel walls, it may be possible to optimize and better understand the process of disrupting the forces that bind cells to surface walls and aggregated cells at filtration pores. RBCs that migrate close to microchannel walls are often attracted by the adhesion force between the RBC and the solid surface originating from the van der Waals forces. Following RBC migration and attachment by adhesive forces adjacent to the microchannel walls as shown in Figure 7, the increase in viscosity at the region causes a lower shear condition and encourages RBC aggregation (cell−cell interaction), which clogs filtering pores or microchannels and reduces flow velocity at filtration region. Both the impact that shear forces and disturbances may induce on cell binding forces with surface walls and other cells leading to aggregation may suggest further characterization. Kinetic parameters such as activation energy and the rate-determining step for cell binding composition attachment and detachment should be considered for modeling the dynamics of RBCs and blood flows under external forces in LOC separation devices.

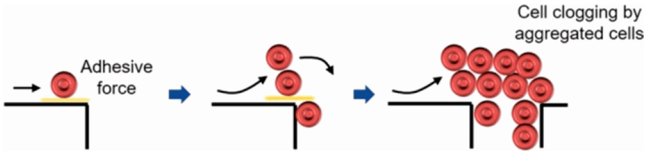

Figure 7. Schematic representations of clogging at a microchannel pore following the sequence of RBC migration, cell attachment to channel walls, and aggregation.[105] Reproduced with permission from ref 105. Copyright 2018 The Authors under the terms of the Creative Commons (CC BY 4.0) License https://creativecommons.org/licenses/by/4.0/.

5.2.3. Relationship between External Forces and Microfluidic Systems. In blood flow, a thicker CFL suggests a lower blood viscosity, suggesting a complex relationship between shear stress and shear rate, affecting the blood viscosity and blood flow. Despite some experimental and numerical studies on electro-osmotic non-Newtonian fluid flow, limited literature has performed an in-depth investigation of the role that applied electric forces and other external forces could play in the process of CFL formation. Additional studies on how shear rates from external forces affect CFL formation and microfluidic flow dynamics can shed light on the mechanism of the contribution induced by external driving forces to the development of a separate phase of layer, similar to CFL, close to the microchannel walls and distinct from the surrounding fluid within the system, then influencing microfluidic flow dynamics.

One of the mechanisms of phenomena to be explored is the formation of the Exclusion Zone (EZ) region following a "Self-Induced Flow" (SIF) phenomenon discovered by Li and Pollack,[106] as shown in Figure 8(a) and (b), respectively. A spontaneous sustained axial flow is observed when hydrophilic materials are immersed in water, resulting in the buildup of a negative layer of charges, defined as the EZ, after water molecules absorb infrared radiation (IR) energy and break down into H^+ and OH^-.

Despite the finding of such a phenomenon, the specific mechanism and role of IR energy have yet to be defined for the process of EZ development. To further develop an understanding of the role of IR energy in such phenomena, a feasible study may be seen through the lens of the relationships between external forces and microfluidic flow. In the phenomena, the increase of SIF velocity under a rise of IR radiation resonant characteristics is shown in the participation of the external electric field near the microchannel walls under electro-osmotic viscoelastic fluid flow systems. The buildup of negative charges at the hydrophilic surfaces in EZ is analogous to the mechanism of electrical double layer formation. Indeed, research has initiated the exploration of the core mechanisms for EZ formation through the lens of the electrokinetic phenomena.[107] Such a similarity of the role of IR energy and the transport phenomena of SIF with electrokinetic phenom-

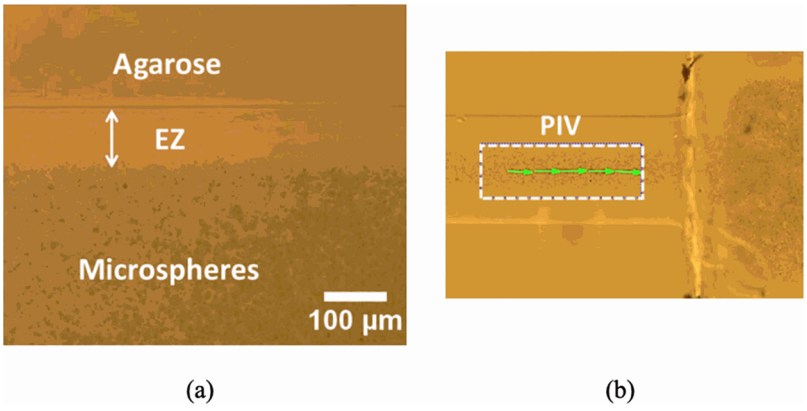

Figure 8. Schematic representations of (a) the Exclusion Zone region and (b) the Self Induced Flow through visualization of microsphere movement within a microchannel.[106] Reproduced with permission from ref 106. Copyright 2020 The Authors under the terms of the Creative Commons (CC BY 4.0) License https://creativecommons.org/licenses/by/4.0/.

https://doi.org/10.1021/cbe.3c00014
Chem Bio Eng. 2024, 1, 26−43

ena paves the way for the definition of the unknown SIF phenomena and EZ formation. Furthermore, Li and Pollack[106] suggest whether CFL formation might contribute to a SIF of blood using solely IR radiation, a commonly available source of energy in nature, as an external driving force. The proposition may be proven feasible with the presence of the CFL region next to the negatively charged hydrophilic endothelial glycocalyx layer, coating the luminal side of blood vessels.[108] Further research can dive into the resonating characteristics between the formation of the CFL region next to the hydrophilic endothelial glycocalyx layer and that of the EZ formation close to hydrophilic microchannel walls. Indeed, an increase in IR energy is known to rapidly accelerate EZ formation and SIF velocity, depicting similarity to the increase in the magnitude of electric field forces and greater shear rates at microchannel walls affecting CFL formation and EOF velocity. Such correlation depicts a future direction in whether SIF blood flow can be observed and characterized theoretically further through the lens of the relationship between blood flow and shear forces exhibited by external energy.

The intricate link between the CFL and external forces, more specifically the externally applied electric field, can receive further attention to provide a more complete framework for the mechanisms between IR radiation and EZ formation. Such characterization may also contribute to a greater comprehension of the role IR can play in CFL formation next to the endothelial glycocalyx layer as well as its role as a driving force to propel blood flow, similar to the SIF, but without the commonly assumed pressure force from heart contraction as a source of driving force.

5.3. Challenges. Although there have been significant improvements in blood flow modeling under LOC systems over the past decade, there are still notable constraints that may require special attention for numerical simulation applications to benefit the adaptability of the designs and functionalities of LOC devices. Several points that require special attention are mentioned below:

1. The majority of CFD models operate under the relationship between the viscoelasticity of blood and the shear rate conditions of flow. The relative effect exhibited by the presence of highly populated RBCs in whole blood and their forces amongst the cells themselves under complex flows often remains unclearly defined. Furthermore, the full range of cell populations in whole blood requires a much more computational load for numerical modeling. Therefore, a vital goal for future research is to evaluate a reduced modeling method where the impact of cell−cell interaction on the viscoelastic property of blood is considered.
2. Current computational methods on hemodynamics rely on continuum models based upon non-Newtonian rheology at the macroscale rather than at molecular and cellular levels. Careful considerations should be made for the development of a constructive framework for the physical and temporal scales of micro/nanoscale systems to evaluate the intricate relationship between fluid driving forces, dynamic viscosity, and elasticity.
3. Viscoelastic fluids under the impact of externally applied electric forces often deviate from the assumptions of no-slip boundary conditions due to the unique flow conditions induced by externally applied forces. Furthermore, the mechanism of vortex formation and viscoelastic flow instability at laminar flow conditions should be better defined through the lens of the microfluidic flow phenomenon to optimize the prediction of viscoelastic flow across different geometrical layouts. Mathematical models and numerical methods are needed to better predict such disturbance caused by external forces and the viscoelasticity of fluids at such a small scale.
4. Under practical situations, zeta potential distribution at channel walls frequently deviates from the common assumption of a constant distribution because of manufacturing faults or inherent surface charges prior to the introduction of electrokinetic influence. These discrepancies frequently lead to inconsistent surface potential distribution, such as excess positive ions at relatively more negatively charged walls. Accordingly, unpredicted vortex formation and flow instability may occur. Therefore, careful consideration should be given to these discrepancies and how they could trigger the transport process and unexpected results of a microdevice.

AUTHOR INFORMATION

Corresponding Authors

Zhe Chen − *Department of Chemical Engineering, School of Chemistry and Chemical Engineering, State Key Laboratory of Metal Matrix Composites, Shanghai Jiao Tong University, Shanghai 200240, P. R. China*; Email: zaccooky@sjtu.edu.cn

Bo Ouyang − *Department of Chemical Engineering, School of Chemistry and Chemical Engineering, State Key Laboratory of Metal Matrix Composites, Shanghai Jiao Tong University, Shanghai 200240, P. R. China*; Email: bouy93@sjtu.edu.cn

Zheng-Hong Luo − *Department of Chemical Engineering, School of Chemistry and Chemical Engineering, State Key Laboratory of Metal Matrix Composites, Shanghai Jiao Tong University, Shanghai 200240, P. R. China*; orcid.org/0000-0001-9011-6020; Phone: +86-21-54745602; Email: luozh@sjtu.edu.cn; Fax: +86-21-54745602

Authors

Bin-Jie Lai − *Department of Chemical Engineering, School of Chemistry and Chemical Engineering, State Key Laboratory of Metal Matrix Composites, Shanghai Jiao Tong University, Shanghai 200240, P. R. China*; orcid.org/0009-0002-8133-5381

Li-Tao Zhu − *Department of Chemical Engineering, School of Chemistry and Chemical Engineering, State Key Laboratory of Metal Matrix Composites, Shanghai Jiao Tong University, Shanghai 200240, P. R. China*; orcid.org/0000-0001-6514-8864

Complete contact information is available at: https://pubs.acs.org/10.1021/cbe.3c00014

Notes

The authors declare no competing financial interest.

ACKNOWLEDGMENTS

This work was supported by the National Natural Science Foundation of China (No. 22238005) and the Postdoctoral Research Foundation of China (No. GZC20231576).

VOCABULARY

Microfluidics: the field of technological and scientific study that investigates fluid flow in channels with dimensions between 1 and 1000 μm

Lab-on-a-Chip Technology: the field of research and technological development aimed at integrating the micro/nanofluidic characteristics to conduct laboratory processes on handheld devices

Computational Fluid Dynamics (CFD): the method utilizing computational abilities to predict physical fluid flow behaviors mathematically through solving the governing equations of corresponding fluid flows

Shear Rate: the rate of change in velocity where one layer of fluid moves past the adjacent layer

Viscoelasticity: the property holding both elasticity and viscosity characteristics relying on the magnitude of applied shear stress and time-dependent strain

Electro-osmosis: the flow of fluid under an applied electric field when charged solid surface is in contact with the bulk fluid

Vortex: the rotating motion of a fluid revolving an axis line

REFERENCES

(1) Neethirajan, S.; Kobayashi, I.; Nakajima, M.; Wu, D.; Nandagopal, S.; Lin, F. Microfluidics for food, agriculture and biosystems industries. *Lab Chip* **2011**, *11* (9), 1574−1586.

(2) Whitesides, G. M. The origins and the future of microfluidics. *Nature* **2006**, *442* (7101), 368−373.

(3) Burklund, A.; Tadimety, A.; Nie, Y.; Hao, N.; Zhang, J. X. J. *Chapter One - Advances in diagnostic microfluidics*; Elsevier, 2020; DOI: DOI: 10.1016/bs.acc.2019.08.001.

(4) Abdulbari, H. A. Chapter 12 - Lab-on-a-chip for analysis of blood. In *Nanotechnology for Hematology, Blood Transfusion, and Artificial Blood*; Denizli, A., Nguyen, T. A., Rajan, M., Alam, M. F., Rahman, K., Eds.; Elsevier, 2022; pp 265−283.

(5) Vladisavljević, G. T.; Khalid, N.; Neves, M. A.; Kuroiwa, T.; Nakajima, M.; Uemura, K.; Ichikawa, S.; Kobayashi, I. Industrial lab-on-a-chip: Design, applications and scale-up for drug discovery and delivery. *Advanced Drug Delivery Reviews* **2013**, *65* (11), 1626−1663.

(6) Kersaudy-Kerhoas, M.; Dhariwal, R.; Desmulliez, M. P. Y.; Jouvet, L. Hydrodynamic blood plasma separation in microfluidic channels. *Microfluid. Nanofluid.* **2010**, *8* (1), 105−114.

(7) Popel, A. S.; Johnson, P. C. Microcirculation and Hemorheology. *Annu. Rev. Fluid Mech.* **2005**, *37* (1), 43−69.

(8) Fedosov, D. A.; Peltomäki, M.; Gompper, G. Deformation and dynamics of red blood cells in flow through cylindrical microchannels. *Soft Matter* **2014**, *10* (24), 4258−4267.

(9) Chakraborty, S. Dynamics of capillary flow of blood into a microfluidic channel. *Lab Chip* **2005**, *5* (4), 421−430.

(10) Tomaiuolo, G.; Guido, S. Start-up shape dynamics of red blood cells in microcapillary flow. *Microvascular Research* **2011**, *82* (1), 35−41.

(11) Sherwood, J. M.; Dusting, J.; Kaliviotis, E.; Balabani, S. The effect of red blood cell aggregation on velocity and cell-depleted layer characteristics of blood in a bifurcating microchannel. *Biomicrofluidics* **2012**, *6* (2), 24119.

(12) Nader, E.; Skinner, S.; Romana, M.; Fort, R.; Lemonne, N.; Guillot, N.; Gauthier, A.; Antoine-Jonville, S.; Renoux, C.; Hardy-Dessources, M.-D. Blood Rheology: Key Parameters, Impact on Blood Flow, Role in Sickle Cell Disease and Effects of Exercise. *Frontiers in Physiology* **2019**, *10*, 01329.

(13) Trejo-Soto, C.; Lázaro, G. R.; Pagonabarraga, I.; Hernández-Machado, A. Microfluidics Approach to the Mechanical Properties of Red Blood Cell Membrane and Their Effect on Blood Rheology. *Membranes* **2022**, *12* (2), 217.

(14) Wagner, C.; Steffen, P.; Svetina, S. Aggregation of red blood cells: From rouleaux to clot formation. *Comptes Rendus Physique* **2013**, *14* (6), 459−469.

(15) Kim, H.; Zhbanov, A.; Yang, S. Microfluidic Systems for Blood and Blood Cell Characterization. *Biosensors* **2023**, *13* (1), 13.

(16) Fåhræus, R.; Lindqvist, T. THE VISCOSITY OF THE BLOOD IN NARROW CAPILLARY TUBES. *American Journal of Physiology-Legacy Content* **1931**, *96* (3), 562−568.

(17) Ascolese, M.; Farina, A.; Fasano, A. The Fåhræus-Lindqvist effect in small blood vessels: how does it help the heart? *J. Biol. Phys.* **2019**, *45* (4), 379−394.

(18) Bento, D.; Fernandes, C. S.; Miranda, J. M.; Lima, R. In vitro blood flow visualizations and cell-free layer (CFL) measurements in a microchannel network. *Experimental Thermal and Fluid Science* **2019**, *109*, 109847.

(19) Namgung, B.; Ong, P. K.; Wong, Y. H.; Lim, D.; Chun, K. J.; Kim, S. A comparative study of histogram-based thresholding methods for the determination of cell-free layer width in small blood vessels. *Physiological Measurement* **2010**, *31* (9), N61.

(20) Hymel, S. J.; Lan, H.; Fujioka, H.; Khismatullin, D. B. Cell trapping in Y-junction microchannels: A numerical study of the bifurcation angle effect in inertial microfluidics. *Phys. Fluids (1994)* **2019**, *31* (8), 082003.

(21) Li, X.; Popel, A. S.; Karniadakis, G. E. Blood-plasma separation in Y-shaped bifurcating microfluidic channels: a dissipative particle dynamics simulation study. *Phys. Biol.* **2012**, *9* (2), 026010.

(22) Yin, X.; Thomas, T.; Zhang, J. Multiple red blood cell flows through microvascular bifurcations: Cell free layer, cell trajectory, and hematocrit separation. *Microvascular Research* **2013**, *89*, 47−56.

(23) Shibeshi, S. S.; Collins, W. E. The Rheology of Blood Flow in a Branched Arterial System. *Appl. Rheol* **2005**, *15* (6), 398−405.

(24) Sequeira, A.; Janela, J. An Overview of Some Mathematical Models of Blood Rheology. In *A Portrait of State-of-the-Art Research at the Technical University of Lisbon*; Pereira, M. S., Ed.; Springer Netherlands: Dordrecht, 2007; pp 65−87.

(25) Walburn, F. J.; Schneck, D. J. A constitutive equation for whole human blood. *Biorheology* **1976**, *13*, 201−210.

(26) Quemada, D. A rheological model for studying the hematocrit dependence of red cell-red cell and red cell-protein interactions in blood. *Biorheology* **1981**, *18*, 501−516.

(27) Varchanis, S.; Dimakopoulos, Y.; Wagner, C.; Tsamopoulos, J. How viscoelastic is human blood plasma? *Soft Matter* **2018**, *14* (21), 4238−4251.

(28) Apostolidis, A. J.; Moyer, A. P.; Beris, A. N. Non-Newtonian effects in simulations of coronary arterial blood flow. *J. Non-Newtonian Fluid Mech.* **2016**, *233*, 155−165.

(29) Luo, X. Y.; Kuang, Z. B. A study on the constitutive equation of blood. *J. Biomech.* **1992**, *25* (8), 929−934.

(30) Oldroyd, J. G.; Wilson, A. H. On the formulation of rheological equations of state. *Proceedings of the Royal Society of London. Series A. Mathematical and Physical Sciences* **1950**, *200* (1063), 523−541.

(31) Prado, G.; Farutin, A.; Misbah, C.; Bureau, L. Viscoelastic transient of confined red blood cells. *Biophys J.* **2015**, *108* (9), 2126−2136.

(32) Huang, C. R.; Pan, W. D.; Chen, H. Q.; Copley, A. L. Thixotropic properties of whole blood from healthy human subjects. *Biorheology* **1987**, *24* (6), 795−801.

(33) Anand, M.; Kwack, J.; Masud, A. A new generalized Oldroyd-B model for blood flow in complex geometries. *International Journal of Engineering Science* **2013**, *72*, 78−88.

(34) Horner, J. S.; Armstrong, M. J.; Wagner, N. J.; Beris, A. N. Investigation of blood rheology under steady and unidirectional large amplitude oscillatory shear. *J. Rheol.* **2018**, *62* (2), 577−591.

(35) Horner, J. S.; Armstrong, M. J.; Wagner, N. J.; Beris, A. N. Measurements of human blood viscoelasticity and thixotropy under steady and transient shear and constitutive modeling thereof. *J. Rheol.* **2019**, *63* (5), 799−813.

https://doi.org/10.1021/cbe.3c00014
Chem Bio Eng. 2024, 1, 26−43

(36) Armstrong, M.; Tussing, J. A methodology for adding thixotropy to Oldroyd-8 family of viscoelastic models for characterization of human blood. *Phys. Fluids* **2020**, *32* (9), 094111.
(37) Crank, J.; Nicolson, P. A practical method for numerical evaluation of solutions of partial differential equations of the heat-conduction type. *Mathematical Proceedings of the Cambridge Philosophical Society* **1947**, *43* (1), 50−67.
(38) Clough, R. W. Original formulation of the finite element method. *Finite Elements in Analysis and Design* **1990**, *7* (2), 89−101.
(39) Liu, W. K.; Liu, Y.; Farrell, D.; Zhang, L.; Wang, X. S.; Fukui, Y.; Patankar, N.; Zhang, Y.; Bajaj, C.; Lee, J.; et al. Immersed finite element method and its applications to biological systems. *Computer Methods in Applied Mechanics and Engineering* **2006**, *195* (13), 1722−1749.
(40) Lopes, D.; Agujetas, R.; Puga, H.; Teixeira, J.; Lima, R.; Alejo, J. P.; Ferrera, C. Analysis of finite element and finite volume methods for fluid-structure interaction simulation of blood flow in a real stenosed artery. *International Journal of Mechanical Sciences* **2021**, *207*, 106650.
(41) Favero, J. L.; Secchi, A. R.; Cardozo, N. S. M.; Jasak, H. Viscoelastic flow analysis using the software OpenFOAM and differential constitutive equations. *J. Non-Newtonian Fluid Mech.* **2010**, *165* (23), 1625−1636.
(42) Pimenta, F.; Alves, M. A. Stabilization of an open-source finite-volume solver for viscoelastic fluid flows. *J. Non-Newtonian Fluid Mech.* **2017**, *239*, 85−104.
(43) Chee, C. Y.; Lee, H. P.; Lu, C. Using 3D fluid-structure interaction model to analyse the biomechanical properties of erythrocyte. *Phys. Lett. A* **2008**, *372* (9), 1357−1362.
(44) Xu, D.; Kaliviotis, E.; Munjiza, A.; Avital, E.; Ji, C.; Williams, J. Large scale simulation of red blood cell aggregation in shear flows. *J. Biomech.* **2013**, *46* (11), 1810−1817.
(45) Johnson, K. L.; Kendall, K.; Roberts, A. Surface energy and the contact of elastic solids. *Proceedings of the royal society of London. A. mathematical and physical sciences* **1971**, *324* (1558), 301−313.
(46) Shi, L.; Pan, T.-W.; Glowinski, R. Deformation of a single red blood cell in bounded Poiseuille flows. *Phys. Rev. E* **2012**, *85* (1), 016307.
(47) Yoon, D.; You, D. Continuum modeling of deformation and aggregation of red blood cells. *J. Biomech.* **2016**, *49* (11), 2267−2279.
(48) Mainardi, F.; Spada, G. Creep, relaxation and viscosity properties for basic fractional models in rheology. *European Physical Journal Special Topics* **2011**, *193* (1), 133−160.
(49) Gracka, M.; Lima, R.; Miranda, J. M.; Student, S.; Melka, B.; Ostrowski, Z. Red blood cells tracking and cell-free layer formation in a microchannel with hyperbolic contraction: A CFD model validation. *Computer Methods and Programs in Biomedicine* **2022**, *226*, 107117.
(50) Aryan, H.; Beigzadeh, B.; Siavashi, M. Euler-Lagrange numerical simulation of improved magnetic drug delivery in a three-dimensional CT-based carotid artery bifurcation. *Computer Methods and Programs in Biomedicine* **2022**, *219*, 106778.
(51) Czaja, B.; Závodszky, G.; Azizi Tarksalooyeh, V.; Hoekstra, A. G. Cell-resolved blood flow simulations of saccular aneurysms: effects of pulsatility and aspect ratio. *J. R Soc. Interface* **2018**, *15* (146), 20180485.
(52) Rydquist, G.; Esmaily, M. A cell-resolved, Lagrangian solver for modeling red blood cell dynamics in macroscale flows. *J. Comput. Phys.* **2022**, *461*, 111204.
(53) Dadvand, A.; Baghalnezhad, M.; Mirzaee, I.; Khoo, B. C.; Ghoreishi, S. An immersed boundary-lattice Boltzmann approach to study the dynamics of elastic membranes in viscous shear flows. *Journal of Computational Science* **2014**, *5* (5), 709−718.
(54) Krüger, T.; Holmes, D.; Coveney, P. V. Deformability-based red blood cell separation in deterministic lateral displacement devices—A simulation study. *Biomicrofluidics* **2014**, *8* (5), 054114.
(55) Takeishi, N.; Ito, H.; Kaneko, M.; Wada, S. Deformation of a Red Blood Cell in a Narrow Rectangular Microchannel. *Micromachines* **2019**, *10* (3), 199.
(56) Krüger, T.; Varnik, F.; Raabe, D. Efficient and accurate simulations of deformable particles immersed in a fluid using a combined immersed boundary lattice Boltzmann finite element method. *Computers & Mathematics with Applications* **2011**, *61* (12), 3485−3505.
(57) Balachandran Nair, A. N.; Pirker, S.; Umundum, T.; Saeedipour, M. A reduced-order model for deformable particles with application in bio-microfluidics. *Computational Particle Mechanics* **2020**, *7* (3), 593−601.
(58) Balachandran Nair, A. N.; Pirker, S.; Saeedipour, M. Resolved CFD-DEM simulation of blood flow with a reduced-order RBC model. *Computational Particle Mechanics* **2022**, *9* (4), 759−774.
(59) Mittal, R.; Iaccarino, G. IMMERSED BOUNDARY METHODS. *Annu. Rev. Fluid Mech.* **2005**, *37* (1), 239−261.
(60) Piquet, A.; Roussel, O.; Hadjadj, A. A comparative study of Brinkman penalization and direct-forcing immersed boundary methods for compressible viscous flows. *Computers & Fluids* **2016**, *136*, 272−284.
(61) Akerkouch, L.; Le, T. B. A Hybrid Continuum-Particle Approach for Fluid-Structure Interaction Simulation of Red Blood Cells in Fluid Flows. *Fluids* **2021**, *6* (4), 139.
(62) Barker, A. T.; Cai, X.-C. Scalable parallel methods for monolithic coupling in fluid-structure interaction with application to blood flow modeling. *J. Comput. Phys.* **2010**, *229* (3), 642−659.
(63) Cetin, A.; Sahin, M. A monolithic fluid-structure interaction framework applied to red blood cells. *International Journal for Numerical Methods in Biomedical Engineering* **2019**, *35* (2), No. e3171.
(64) Freund, J. B. Numerical Simulation of Flowing Blood Cells. *Annu. Rev. Fluid Mech.* **2014**, *46* (1), 67−95.
(65) Ye, T.; Phan-Thien, N.; Lim, C. T. Particle-based simulations of red blood cells—A review. *J. Biomech.* **2016**, *49* (11), 2255−2266.
(66) Arabghahestani, M.; Poozesh, S.; Akafuah, N. K. Advances in Computational Fluid Mechanics in Cellular Flow Manipulation: A Review. *Applied Sciences* **2019**, *9* (19), 4041.
(67) Rathnayaka, C. M.; From, C. S.; Geekiyanage, N. M.; Gu, Y. T.; Nguyen, N. T.; Sauret, E. Particle-Based Numerical Modelling of Liquid Marbles: Recent Advances and Future Perspectives. *Archives of Computational Methods in Engineering* **2022**, *29* (5), 3021−3039.
(68) Li, X.; Vlahovska, P. M.; Karniadakis, G. E. Continuum- and particle-based modeling of shapes and dynamics of red blood cells in health and disease. *Soft Matter* **2013**, *9* (1), 28−37.
(69) Beris, A. N.; Horner, J. S.; Jariwala, S.; Armstrong, M. J.; Wagner, N. J. Recent advances in blood rheology: a review. *Soft Matter* **2021**, *17* (47), 10591−10613.
(70) Arciero, J.; Causin, P.; Malgaroli, F. Mathematical methods for modeling the microcirculation. *AIMS Biophysics* **2017**, *4* (3), 362−399.
(71) Maria, M. S.; Chandra, T. S.; Sen, A. K. Capillary flow-driven blood plasma separation and on-chip analyte detection in microfluidic devices. *Microfluid. Nanofluid.* **2017**, *21* (4), 72.
(72) Huhtamäki, T.; Tian, X.; Korhonen, J. T.; Ras, R. H. A. Surface-wetting characterization using contact-angle measurements. *Nat. Protoc.* **2018**, *13* (7), 1521−1538.
(73) Young, T., III. An essay on the cohesion of fluids. *Philosophical Transactions of the Royal Society of London* **1805**, *95*, 65−87.
(74) Kim, Y. C.; Kim, S.-H.; Kim, D.; Park, S.-J.; Park, J.-K. Plasma extraction in a capillary-driven microfluidic device using surfactant-added poly(dimethylsiloxane). *Sens. Actuators, B* **2010**, *145* (2), 861−868.
(75) Washburn, E. W. The Dynamics of Capillary Flow. *Physical Review* **1921**, *17* (3), 273−283.
(76) Cito, S.; Ahn, Y. C.; Pallares, J.; Duarte, R. M.; Chen, Z.; Madou, M.; Katakis, I. Visualization and measurement of capillary-driven blood flow using spectral domain optical coherence tomography. *Microfluid Nanofluidics* **2012**, *13* (2), 227−237.
(77) Berthier, E.; Dostie, A. M.; Lee, U. N.; Berthier, J.; Theberge, A. B. Open Microfluidic Capillary Systems. *Anal Chem.* **2019**, *91* (14), 8739−8750.

https://doi.org/10.1021/cbe.3c00014
Chem Bio Eng. 2024, 1, 26−43

(78) Berthier, J.; Brakke, K. A.; Furlani, E. P.; Karampelas, I. H.; Poher, V.; Gosselin, D.; Cubizolles, M.; Pouteau, P. Whole blood spontaneous capillary flow in narrow V-groove microchannels. *Sens. Actuators, B* **2015**, *206*, 258−267.
(79) Hirt, C. W.; Nichols, B. D. Volume of fluid (VOF) method for the dynamics of free boundaries. *J. Comput. Phys.* **1981**, *39* (1), 201−225.
(80) Chen, J.-L.; Shih, W.-H.; Hsieh, W.-H. AC electro-osmotic micromixer using a face-to-face, asymmetric pair of planar electrodes. *Sens. Actuators, B* **2013**, *188*, 11−21.
(81) Zhao, C.; Yang, C. Electrokinetics of non-Newtonian fluids: A review. *Advances in Colloid and Interface Science* **2013**, *201-202*, 94−108.
(82) Oh, K. W. 6 - Lab-on-chip (LOC) devices and microfluidics for biomedical applications. In *MEMS for Biomedical Applications*; Bhansali, S., Vasudev, A., Eds.; Woodhead Publishing, 2012; pp 150−171.
(83) Bello, M. S.; De Besi, P.; Rezzonico, R.; Righetti, P. G.; Casiraghi, E. Electroosmosis of polymer solutions in fused silica capillaries. *ELECTROPHORESIS* **1994**, *15* (1), 623−626.
(84) Park, H. M.; Lee, W. M. Effect of viscoelasticity on the flow pattern and the volumetric flow rate in electroosmotic flows through a microchannel. *Lab Chip* **2008**, *8* (7), 1163−1170.
(85) Afonso, A. M.; Alves, M. A.; Pinho, F. T. Analytical solution of mixed electro-osmotic/pressure driven flows of viscoelastic fluids in microchannels. *J. Non-Newtonian Fluid Mech.* **2009**, *159* (1), 50−63.
(86) Sousa, J. J.; Afonso, A. M.; Pinho, F. T.; Alves, M. A. Effect of the skimming layer on electro-osmotic—Poiseuille flows of viscoelastic fluids. *Microfluid. Nanofluid.* **2011**, *10* (1), 107−122.
(87) Zhao, C.; Yang, C. Electro-osmotic mobility of non-Newtonian fluids. *Biomicrofluidics* **2011**, *5* (1), 014110.
(88) Pimenta, F.; Alves, M. A. Electro-elastic instabilities in cross-shaped microchannels. *J. Non-Newtonian Fluid Mech.* **2018**, *259*, 61−77.
(89) Bezerra, W. S.; Castelo, A.; Afonso, A. M. Numerical Study of Electro-Osmotic Fluid Flow and Vortex Formation. *Micromachines (Basel)* **2019**, *10* (12), 796.
(90) Ji, J.; Qian, S.; Liu, Z. Electroosmotic Flow of Viscoelastic Fluid through a Constriction Microchannel. *Micromachines (Basel)* **2021**, *12* (4), 417.
(91) Zhao, C.; Yang, C. Exact solutions for electro-osmotic flow of viscoelastic fluids in rectangular micro-channels. *Applied Mathematics and Computation* **2009**, *211* (2), 502−509.
(92) Gerum, R.; Mirzahossein, E.; Eroles, M.; Elsterer, J.; Mainka, A.; Bauer, A.; Sonntag, S.; Winterl, A.; Bartl, J.; Fischer, L. Viscoelastic properties of suspended cells measured with shear flow deformation cytometry. *Elife* **2022**, *11*, e78823.
(93) Sadek, S. H.; Pinho, F. T.; Alves, M. A. Electro-elastic flow instabilities of viscoelastic fluids in contraction/expansion micro-geometries. *J. Non-Newtonian Fluid Mech.* **2020**, *283*, 104293.
(94) Spanjaards, M.; Peters, G.; Hulsen, M.; Anderson, P. Numerical Study of the Effect of Thixotropy on Extrudate Swell. *Polymers* **2021**, *13* (24), 4383.
(95) Rashidi, S.; Bafekr, H.; Valipour, M. S.; Esfahani, J. A. A review on the application, simulation, and experiment of the electrokinetic mixers. *Chemical Engineering and Processing - Process Intensification* **2018**, *126*, 108−122.
(96) Matsubara, K.; Narumi, T. Microfluidic mixing using unsteady electroosmotic vortices produced by a staggered array of electrodes. *Chemical Engineering Journal* **2016**, *288*, 638−647.
(97) Qaderi, A.; Jamaati, J.; Bahiraei, M. CFD simulation of combined electroosmotic-pressure driven micro-mixing in a micro-channel equipped with triangular hurdle and zeta-potential hetero-geneity. *Chemical Engineering Science* **2019**, *199*, 463−477.
(98) Cho, C.-C.; Chen, C.-L.; Chen, C. o.-K. Mixing enhancement in crisscross micromixer using aperiodic electrokinetic perturbing flows. *International Journal of Heat and Mass Transfer* **2012**, *55* (11), 2926−2933.
(99) Zhao, W.; Yang, F.; Wang, K.; Bai, J.; Wang, G. Rapid mixing by turbulent-like electrokinetic microflow. *Chemical Engineering Science* **2017**, *165*, 113−121.
(100) Tran, T.; Chakraborty, P.; Guttenberg, N.; Prescott, A.; Kellay, H.; Goldburg, W.; Goldenfeld, N.; Gioia, G. Macroscopic effects of the spectral structure in turbulent flows. *Nat. Phys.* **2010**, *6* (6), 438−441.
(101) Toner, M.; Irimia, D. Blood-on-a-chip. *Annu. Rev. Biomed Eng.* **2005**, *7*, 77−103.
(102) Maria, M. S.; Rakesh, P. E.; Chandra, T. S.; Sen, A. K. Capillary flow of blood in a microchannel with differential wetting for blood plasma separation and on-chip glucose detection. *Biomicro-fluidics* **2016**, *10* (5), 054108.
(103) Tripathi, S.; Varun Kumar, Y. V. B.; Prabhakar, A.; Joshi, S. S.; Agrawal, A. Passive blood plasma separation at the microscale: a review of design principles and microdevices. *Journal of Micro-mechanics and Microengineering* **2015**, *25* (8), 083001.
(104) Mohammadi, M.; Madadi, H.; Casals-Terré, J. Microfluidic point-of-care blood panel based on a novel technique: Reversible electroosmotic flow. *Biomicrofluidics* **2015**, *9* (5), 054106.
(105) Kang, D. H.; Kim, K.; Kim, Y. J. An anti-clogging method for improving the performance and lifespan of blood plasma separation devices in real-time and continuous microfluidic systems. *Sci. Rep* **2018**, *8* (1), 17015.
(106) Li, Z.; Pollack, G. H. Surface-induced flow: A natural microscopic engine using infrared energy as fuel. *Science Advances* **2020**, *6* (19), No. eaba0941.
(107) Mercado-Uribe, H.; Guevara-Pantoja, F. J.; García-Muñoz, W.; García-Maldonado, J. S.; Méndez-Alcaraz, J. M.; Ruiz-Suárez, J. C. On the evolution of the exclusion zone produced by hydrophilic surfaces: A contracted description. *J. Chem. Phys.* **2021**, *154* (19), 194902.
(108) Yalcin, O.; Jani, V. P.; Johnson, P. C.; Cabrales, P. Implications Enzymatic Degradation of the Endothelial Glycocalyx on the Microvascular Hemodynamics and the Arteriolar Red Cell Free Layer of the Rat Cremaster Muscle. *Front Physiol* **2018**, *9*, 168.

https://doi.org/10.1021/cbe.3c00014
Chem Bio Eng. 2024, 1, 26−43